The build-up and triggers of volcanic eruptions

The build-up to and triggers of volcanic eruptions

Luca Caricchi[1,*], Meredith Townsend[2], Eleonora Rivalta[3], Atsuko Namiki[4]

1) Department of Earth Sciences, University of Geneva, rue des Maraîchers 13, 1205, Geneva, Switzerland
2) Department of Earth Sciences, University of Oregon, 100 Cascade Hall, 1272 Eugene, OR, USA.
3) GeoForschungsZentrum, Helmholtzstraße 6/7, 14467 Potsdam, Germany
4) Graduate School of Environmental Studies, Nagoya University, Furo-cho, Chikusa, Nagoya 464-8601, Japan

email: Luca.Caricchi@unige.ch, mtownse4@uoregon.edu

Abstract

Volcanic eruptions can directly impact more than 800 million people living in proximity to active volcanoes. Thus, anticipating the future behaviour of volcanic systems serves to mitigate the effects of eruptions on our society. Essential to this target is an understanding of the fundamental processes driving volcanic activity. Here, we review the processes leading to magma accumulation in the Earth's crust and the temporal evolution of the thermal and physical properties of magma storage regions. We discuss mechanisms to initiate magma reservoir failure and the ascent of magma from crustal storage regions, including the factors that control whether magma reaches the surface or stalls at depth. We show that the evolution of temperature and the physical properties of volcanic plumbing systems favour volcanic activity after a period of thermal priming, while storage becomes more likely for mature volcanic systems with large reservoirs (hundreds of km^3) when the crust is relatively warm. Anticipating volcanic activity requires a multidisciplinary approach as monitoring and geophysics provide information on the current state of system while petrology and the eruptive history are essential to trace the temporal evolution of volcanic systems over longer timescales. Modelling serves to link these different observational timescales, and the inversion of datasets using physics-based statistical approaches is a promising way forward

to advance our understanding of the processes controlling recurrence rate and magnitude of volcanic eruptions.

1. Introduction

Volcanic eruptions occur when magma reaches or, for some phreatic eruptions, approaches the surface[1,2]. In order to anticipate the timing, size, and style of volcanic eruptions, we need a scientific understanding of magma plumbing systems and the processes that govern the transfer of magma to the surface[3]. Volcanic eruptions are the culmination of a long series of processes that occur in disparate regions of the earth's lithosphere, starting with the generation and supply of melt from the mantle, the accumulation of magma in crustal reservoirs, and the transport of magma between and within storage regions and to the surface (Fig.1). Each of these processes represents a crucial step in the journey of magma to the surface, and in the last few decades we have made considerable progress in understanding particularly the storage and transport of magma through the crust. From these advances, a counterintuitive truth has emerged: it is surprisingly difficult for magma to reach the surface. Volcanic eruptions require a sufficiently large volume of magma with adequately low viscosity and density to reach the surface without totally solidifying en-route[4–10]. However, the assembly and growth of magma reservoirs in the crust requires a supply of heat sufficient to overcome freezing against the host rocks. While this may be easier in the lower crust where more primitive magma reservoirs are thought to form, the development of more silicic reservoirs in the shallow crust likely requires a protracted period of thermal maturation[11,12]. Even if a magma reservoir can be thermally sustained, in order to feed a potential eruption it must build up pressure, although the range of overpressure required is debated[13,14]. External triggers such as earthquakes[15], landslides[16–18], and tides[19] can provide the "final kick" at different time scales to destabilize a magma reservoir, but the small pressure changes

associated with some of these processes require the reservoir to be close to failure to trigger magma ascent. Once magma starts ascending from a reservoir, its ability to reach the surface depends on a wide variety of factors, including: the evolution of physical properties of the magma, which is largely influenced by the behaviour of volatiles[5,20,21] and heat loss to the surrounding rocks[22 18]; the physical properties of the surrounding rocks; and the local stress field, which is influenced by local tectonics and topographic loading of the volcanic edifice[8,23–25]. The reservoir must supply sufficient energy and volume to drive magma to the surface without it becoming thermally or mechanically arrested[26–28]. Many episodes of volcanic unrest that do not culminate in an eruption are thought to represent "failed eruptions" or dike intrusions that became arrested at shallow depths[29]. Considering all the barriers to magma reaching the surface, volcanic eruptions may seem improbable; however, an average of 50 volcanoes erupt every year on Earth[30]. The prevalence of eruptions despite thermal and mechanical obstacles is consistent with a much larger amount of magma emplaced at a depth that never reaches the surface[12,31–36].

In this review, we discuss the processes behind volcanic eruptions following the journey of magma to the surface. Although we focus on eruptions from polygenetic volcanoes with crustal sources, many of the general principles we discuss are applicable to monogenetic volcanoes. We begin with a short summary of observations about volcanic eruption triggers gathered from analyses of erupted products and volcano monitoring signals. Next, we review the processes responsible for magma accumulation, reservoir pressurisation, and the factors that might promote or hinder the propagation of magma to the surface. We close this review by summarising the current challenges to understanding what controls volcanic eruptions and highlighting how multidisciplinary research is key to our endeavour.

2. Magma storage

2.1 Pre- and post-eruption record

We cannot directly observe the long-term (hundreds to hundreds of thousands of years) processes preceding volcanic eruptions both because of their timespan and the inaccessible depths at which these processes occur. Therefore, we rely on monitoring data along with data from the textures and chemistry of erupted materials, as well as field and structural geology to build models for the sequence of events culminating in an eruption. Volcano monitoring is essential to determine the status of volcanic systems and identify the potential signs of an impending eruption. The number of volcanoes for which data are available has recently increased, thanks to the advent of satellite technology and deployment of state-of-the-art ground-based instrumentation[37–45]. Such data availability[46] has opened the way to multi-parametric monitoring and stimulated the comparison between volcanoes[37,38,41,44,47–50].

The chemistry and textures of volcanic rocks contain information about pre- and syn-eruptive processes that are decrypted using experiments (e.g. Refs.[20,51–59]). Combining the investigation of eruptive products and intrusive and eruptive geometries/patterns in the field with the multiparametric monitoring record of recent volcanic eruptions is a promising tool to shed light on the sequence of events leading up to volcanic eruptions[38,43,60–87]. Even considering a highly idealized magmatic plumbing system (Fig. 1), similar monitoring signals and petrologic phenomena may be produced by fundamentally different magmatic processes. For instance, an increase in CO_2-rich or H_2O-rich emissions at the surface could be explained equally well by the release of fluids during magma ascent from depth (e.g. Ref.[88]; Fig. 1a), or by fluid flushing from depth that triggers the release of gases to the surface[89,90] (Fig. 1d). The presence of partially reacted minerals, or groups of minerals of distinct chemistry in volcanic products (Fig. 1b), could be the result of interaction between a hotter, more mafic magma and a colder, more felsic magma, or it could be the product of the interaction between magma and

fluids ascending from depth (e.g. Ref.[58]). Both magma injection and fluid flushing/fluxing (the percolation and chemical interaction between externally sourced magmatic fluids and magma) could drive inflation of the volcanic edifice detected geodetically at the surface and produce similar petrologic signals[91–94]. These considerations highlight the need for a multidisciplinary approach to determine the sequence of events that finally lead to a volcanic eruption.

2.2. Assembly of magma reservoirs

Geologic and geodetic data together with modelling show that the transfer and accumulation of magma in the Earth's crust is not continuous[8,26,95–97]. However, thermal modelling shows that the long-term (hundreds of thousands to millions of years) thermal and physical evolution of magma within crustal plumbing systems can be described by the average rate of magma input[11,12,36,98]. The thermal evolution of volcanic plumbing systems directly impacts the capacity of magmatic systems to feed volcanic activity by controlling the rate of accumulation of eruptible magma and the temporal evolution of the physical properties of magma and rocks surrounding the plumbing system. To illustrate quantitatively these effects we use the thermal modelling results of Ref.[36] simulating the episodic and prolonged input of magma in the crust.

The calculations show that the presence of even a minor amount of exsolved (or excess) volatiles strongly increases magma compressibility[99,100] (Fig. 2a). Magma input into the crust results initially in rapid cooling below its solidus temperature, after which the model reservoir starts growing at a rate proportional to the rate of magma input (Fig. 2b, c). This initial "incubation period" is longer for lower rates of magma input. For the greatest input rate presented here, eruptible magma (defined here as T>750 °C, melt fraction>0.4) starts accumulating after a few hundred thousand years, while for the lowest magma input rate,

127 eruptible magma is sporadically present throughout the 1.5 million years of magma injection
128 in the crust (Fig. 2b, c). For both rates of magma input, compressibility increases rapidly and
129 then reaches a relatively constant value over time (Fig. 2d, e). Once the relatively constant
130 values are achieved, magma compressibility is greater in the reservoir assembled with higher
131 rates of magma input, as it contains a higher fraction of magma above solidus (Fig. 2d, e). To
132 summarise, after a period of time over which eruptible magma is present in extremely small
133 fractions, i.e. the "incubation period[11]", eruptible magma starts to accumulate for relatively
134 high rates of magma input, while is present sporadically for lower rates (Fig. 2b, c). With
135 increasing time, the wall rock temperature increases (i.e. viscosity decreases[12]), as does
136 magma compressibility, both of which decrease the capacity of a magma reservoir to
137 pressurise to values sufficiently high to initiate magma ascent. Moreover, the release of
138 exsolved H_2O-rich fluids results in the variation of the temperature-melt fraction
139 relationships, which, in turn, decreases the capacity of heat (i.e. magma) input to alter the
140 properties of the resident magma[101]. All together, these results suggest that the likelihood of
141 an eruption to occur is lower during the incubation period because of the small amount of
142 eruptible magma available, higher after substantial eruptible volumes accumulate, but then
143 lower again over time once volatiles exsolve and the magma becomes highly compressible[102].
144 However, on the long-term, the accumulation of super-solidus volatile-rich magma leads to a
145 progressive decrease in magma density, and an associated increase of magma buoyancy,
146 which could bring the magmatic system to critical conditions and initiate the release of
147 magma from the reservoir[102–104]. Somewhat counterintuitively, the time window over which
148 eruptions are most likely is shorter for systems assembled at the highest rates of magma input
149 because the temperature of the wall rock and the compressibility of magma increase more
150 rapidly in systems assembled at high rates of magma input. We note that these calculations do
151 not include the possibility of volatile outgassing, which would decrease compressibility over

time[105–107], nor do they include the effects of magma withdrawal from a reservoir (e.g. during an eruption); the removal of mass and heat associated with frequent withdrawal events could inhibit the growth of large magma reservoirs and potentially prolong both the incubation period as well as the period over which a plumbing system feeds volcanic activity[103].

Internal magma reservoir dynamics such as magma mixing, convective overturn, and crystal-melt-volatile phase separations can also influence the rheology, and thus the eruptibility, of magma. If the Rayleigh number is sufficiently high, magma mixing and convective processes may act to homogenize a magma reservoir[108–110], which has been thought to stimulate the exsolution of volatiles if an intruding magma is volatile-rich[111], but could also lead to resorption of volatiles if an intruding magma supplies sufficient heat and pressure[112]. Volatile exsolution can be a driver of mixing processes by altering magma density[113–115], or if volatiles migrate more easily they can act to suppress mixing and melt migration[116,117]. Magma mixing and convective overturn have been invoked as eruption triggers[110,111,118–120], but we note that most physical models for internal magma reservoir dynamics typically do not include mechanical interaction with the surrounding crust, and that this link would be an important target for future work to better understand how mixing processes contribute to reservoir overpressure.

2.3. The “critical overpressure” for magma reservoir failure

Magma transport out of crustal storage zones takes place primarily by fluid-driven fracturing into the surrounding brittle crust, and potentially to the surface[22,121–123]. Depending on the geometry and orientation of these magma-filled fractures, they are referred to as dikes, sills, inclined sheets, cone sheets, or ring dikes[124–126]. Although in detail magma-filled fractures display structural complexities and may even intrude as viscous fingers through poorly-consolidated sediments in the uppermost part of the crust[127], the vast majority of these

177 intrusive structures are approximately planar and dominantly opening-mode fractures[128–130],
178 which we will hereafter refer to as dikes for convenience. The details surrounding the
179 initiation of dikes and their connection to magma chambers are poorly understood, which has
180 led to competing theories about the criteria to initiate a diking event. Because dikes are
181 dominantly opening-mode structures, most magma transport models adopt a criterion based
182 on one of two conditions: (1) *tensile failure* of wall rocks[13,131,132] or (2) the *dilation and*
183 *propagation in pre-existing fractures* driven by magma pressure[102,133–136]. Less commonly,
184 shear failure criteria are included[137,138].

185 *Tensile failure* in otherwise unfractured wall rocks can occur if the stress tangential to
186 the chamber walls $\sigma_{\theta\theta}$, sometimes referred to as the "hoop stress", exceeds the tensile
187 strength of the wall rocks T_s minus the pore-fluid pressure p_w (Box1), using a tension-
188 positive convention:

189 $$\sigma_{\theta\theta} \geq T_{s-} p_w \qquad (1)$$

190 In hydrostatic conditions, $p_w = \rho_w g h$, where ρ_w is the fluid density, g is gravitational
191 acceleration, and h is depth[13,131,139,140]. Laboratory measurements on rocks suggest an average
192 tensile strength of ~0-10 MPa (e.g. Ref.[141]). Elastic models for the stress around spherical
193 magma chambers indicate that the magma overpressure ΔP_{crit} at which the hoop stress
194 becomes tensile is approximately twice the lithostatic pressure[13,142,143]. In other words, for a
195 spherical magma chamber at ~8 km depth or ~200 MPa lithostatic pressure in a homogeneous
196 elastic crust, ΔP_{crit} would be ~400 MPa. Evidence that magmas in shallow crustal reservoirs
197 reach such extreme overpressures is lacking, which suggests that either 1) irregularities along
198 the chamber margins or deviations from a spherical shape act to concentrate stress, leading to
199 tensile fracture at substantially lower overpressures[144,145]; or 2) the host crust is not a
200 homogeneous elastic solid but contains pre-existing weaknesses.

Pre-existing fractures along magma chamber walls may be dilated if the magma pressure exceeds the fracture-normal compressive stress[133,134]. If magma initially invades and pressurizes a pre-existing fracture, it may lead to further fracturing and the creation of new fractures near the tip region that magma can flow into. In other words, these pre-existing fractures may help to weaken the host rock and get the magma initially moving out of the reservoir, but ultimately the magma may still create its own path. In order to propagate a pre-existing fracture of initial length l (Box 1), the magma overpressure must reach:

$$\Delta P_{crit} \geq \frac{K_c}{\sqrt{l}} \qquad (2)$$

where K_c is the fracture toughness of the rock, which may be on the order of ~1-10 MPa $m^{1/2}$ for centimetre- to meter-scale fractures[22,102]. Magma will more easily propagate in longer, suitably oriented pre-existing fractures. The critical overpressure to propagate a fracture that is 1 meter long is only ~1 – 10 MPa (Fig. 3), which is significantly less than that required to create new fractures altogether and therefore a more likely scenario. If wall rocks are weak or fracture toughness is minimal, the critical overpressure may instead be that required to overcome magma freezing against the fracture walls[22] or the viscous resistance of magma to flow through a narrow fracture[8,146].

Viscous deformation of the wall rocks also may influence whether magma reservoir failure can occur (Fig. 3), especially over longer timescales as magma heats up the surrounding rocks or develops a layer of "crystal mush" around the edges of the reservoir (Box 1). This idea has led to the development of magma chamber models that consider a viscoelastic crust[147–149]. Within this framework, we can consider the viscous strain rate in the crust $\dot{\gamma}$ due to a differential stress σ associated with reservoir overpressurisation

$$\dot{\gamma} = A\sigma^n e^{-(Q+PV_a)/(R_g T)} \qquad (3)$$

where T is temperature, P is the mechanical pressure in the wall rocks, Q is the activation energy, V_a is activation volume, R_g is the gas constant, and A depends on the mineralogy of

the wall rock, the minerals' grain size, and water fugacity[150]. Under cold upper crustal conditions and mm-size grains, the stress exponent n>2 is appropriate, which indicates flow in dislocation creep regime[150]. With increasing strain rates, brittle failure becomes more likely, and we can recast the criterion for magma reservoir failure and diking in terms of a critical strain rate $\dot{\gamma}_{crit}$ associated with a critical differential stress σ_{crit} corresponding to the critical magma overpressure ΔP_{crit}:

$$\dot{\gamma}_{crit} = \frac{\sigma_{crit}}{\eta_r} \sim \frac{\Delta P_{crit}}{\eta_r} \equiv \frac{1}{\tau_{relax}} \quad (4)$$

η_r is the effective host-rock viscosity around a magma chamber, and we can see the critical strain rate for diking increases as the host-rock viscosity decreases. This suggests, for example, that magma chamber failure is easier at shallower depths where the ambient host-rock temperature is colder and η_r is greater. The specific relationship between the critical stress σ_{crit} and critical overpressure ΔP_{crit} will be a function of the host rock properties such as temperature, pressure and mineralogy, as well as the magma reservoir properties such as the size and shape of the magma body, and the presence or absence of pre-existing fractures as discussed above. In this formulation, the critical strain rate $\dot{\gamma}_{crit}$ is the inverse of the viscous relaxation timescale τ_{relax} as defined in Ref.[151]. Refs.[100,152–154] use the ratio $\eta_r / \Delta P_{crit}$ to estimate τ_{relax} for magma chambers at various depths, using a calculation of η_r based on the steady-state temperature profile around a magma chamber and assuming that ΔP_{crit} has to be at least that required to propagate pre-existing fractures (Equation 2). For example, if we apply the calculation of η_r from Ref.[151], we find that a depth range between ~10 – 6 km corresponds to η_r of ~10^{19} – 10^{21} Pa·s for the crust around a magma chamber at 850 °C. Using ΔP_{crit} of 20 MPa, $\dot{\gamma}_{crit} \sim \frac{1}{\tau_{relax}}$ ranges from 60 myr^{-1} – 0.6 myr^{-1}. In the next section, we review processes that give rise to magma overpressure and strain in the wall rocks, and we evaluate how they compare to $\dot{\gamma}_{crit}$.

3. Magma pressurization/eruption triggering

3.1 Internal triggers

3.1.1 Magma recharge

Geophysical, geochemical, and petrological evidence support the hypothesis that magma injection from deeper sources to shallow crustal chambers can lead to volcanic eruptions (e.g. Refs.[44,86,111]). For example, magma injection has been invoked as a trigger for the eruption of Pinatubi in 1991[67] and the 3.6 ka Bronze Age eruption of Santorini[155]. The accumulation of magma in crustal reservoirs can cause ground inflation that can be detected geodetically[38,156,157]. Ground inflation usually precedes volcanic eruptions, although in some cases eruptions have occurred without any preceding measured ground deformation, and episodes of inflation often occur in active volcanic settings without culminating in eruption[158]. In some cases, uplift over longer (1-10 kyr) timescales is recorded in geomorphic features (e.g. Refs.[159,160]) indicating that magma recharge and accumulation may occur episodically over thousands of years, incrementally increasing the magma reservoir volume and potentially the overpressure. The addition of new magma or volatiles to a shallow reservoir also may stimulate gas emissions and increase surface heat flow, another sign of potential unrest[161,162]. In the rock record, the interaction of hotter mafic magmas with resident silicic magmas may be recorded in plutonic settings as microgranular enclaves and magma mingling structures that form in layered intrusions[120,163–165], as well as in the geochemistry and textures of volcanic products (Fig. 1b). Crystals record chemical variations from core to rim that can be deconvolved to identify the addition of more mafic and hotter magma into a colder, more silicic reservoir[166–169]. Additional information about the timescales of recharge and mixing events can be extracted from chemical profiles in minerals providing the

opportunity to link pre-eruptive monitoring signals to the processes that ultimately led to an eruption[76,82,170].

Physical models can provide a theoretical framework to determine the conditions under which magma recharge may trigger an eruption[102,136,151,171–173]. Whether or not magma recharge leads to the critical overpressure required for reservoir failure depends on the magnitude, rate, and style of magma recharge, the current pressure in the reservoir, magma compressibility (Fig. 2d, e), and the rate at which pressure may be relaxed by viscous or plastic deformation of the wall rocks. If the host rock is purely elastic, i.e. if the magma recharge occurs faster than the timescale for viscous deformation, the increase in pressure in the reservoir ΔP due to an increase in magma volume ΔV is approximately $\Delta P = \frac{\Delta V}{V}\beta^{-1}$ (Box 1), where β is the sum of magma and reservoir compressibility[148]. Hence, in a purely elastic crust, the potential for recharge to trigger an eruption decreases for increasing reservoir volume and compressibility[153]. Over timescales approaching and exceeding the timescale for viscous deformation of the crust (Eq. 4), pressure can be relaxed by deformation of the wall rocks (e.g. Ref.[147]). To explore whether magma recharge can build up critical overpressure over these longer timescales, we can considered the strain rate $\dot{\gamma}_{in}$ associated with the rate of magma injection $\dot{V}_{in}$ [102,103,136,151]

$$\dot{\gamma}_{in} = \frac{\dot{V}_{in}}{V} \equiv \frac{1}{\tau_{in}} \quad (5)$$

We note that $\dot{\gamma}_{in}$ is the inverse of the injection timescale τ_{in} of Ref.[151]. Thus, on timescales over which viscous relaxation is expected to be important, recharge may trigger the release of magma from a reservoir if $\dot{\gamma}_{in} > \dot{\gamma}_{crit}$ (Eq. 4).

To estimate $\dot{\gamma}_{in}$ for natural systems we need constraints on the magma injection rate and the total volume of the magma chamber being recharged, neither of which can be measured directly. Eruptive rates are commonly used as a proxy for magma supply rates (e.g.,

298 Refs.[81,100]), although this requires making assumptions about the ratio of magma intruded to
299 erupted[35,81]. The volume of a magma chamber can be estimated from geophysical imaging
300 such as gravity or magnetotellurics[174,175], or from eruptive volumes, as models for effusive
301 eruptions suggest that the volume erupted scales as ~1 – 10% of the chamber volume[27,176].
302 One exceptional example where both the magma chamber volume and supply rate have been
303 relatively well constrained is Laguna del Maule in the southern Andes. Based on the
304 combination of eruptive flux and inflation of the volcano over the Holocene, the magma
305 supply rate is estimated at ~0.0023 km^3/yr[159]. A gravity survey by Ref.[174] indicated a melt-
306 rich magma body ~30 km^3 in volume located under the caldera. Together, this leads to
307 $\dot{\gamma}_{in}$~76 myr^{-1}, which is faster than our estimates of $\dot{\gamma}_{crit}$ in Section 2.3, which suggests that
308 the Holocene phase of eruptive activity at Laguna del Maule likely was triggered by magma
309 injection to a shallow crustal chamber.
310
311 3*.1.2 The role of volatile exsolution*
312 Magma cooling and crystallisation can increase the concentration of magmatic H_2O
313 and CO_2 in the residual melt, which may eventually trigger the exsolution of a low-density,
314 relatively compressible magmatic volatile phase e.g. Ref.[90]. This process, commonly referred
315 to as "second boiling," can increase pressure in a magma reservoir and has been invoked as a
316 potential eruption trigger (e.g. Calbuco 2015[177] and Kelud 2014[178] eruptions). Another
317 mechanism that may stimulate volatile exsolution is the "flushing" or addition and chemical
318 interaction of deeply sourced magmatic fluids with magma stored at shallower depths[89].
319 Erupted products might provide sufficient information to identify whether crystallization-
320 induced degassing or volatile flushing ultimately initiated the propagation of magma toward
321 the surface. Melt inclusions are used to trace the evolution of volatiles in magmatic systems
322 and can in principle be used to discern crystallisation-induced degassing and

flushing[89,93,179,180]; however, potential issues linked to post-entrapment processes should be carefully considered before applying this method[179,181,182]. Apatite is a promising proxy to trace the processes responsible for the presence of excess fluids and their chemistry in magmatic systems[52,71,183,184]. While both crystallisation-induced degassing and flushing are associated with magma crystallisation, in the first case the water activity in the melt increases, and in the second it decreases, which implies that the phase equilibria and the chemical evolution of the residual melt fraction will differ (e.g. Refs.[58,59]). Thus, these two processes could be discerned also using major and trace element chemistry of major mineral phases.

Geophysical observations of volatile exsolution may be cryptic because the high compressibility of the volatile phase may suppress surface deformation[43,99]. In addition, because the rate of volatile exsolution is linked to magma's cooling rate, this process may result in the increase of magma volume over timescales that are longer than the viscous relaxation of the crust and therefore do not generate overpressure (Fig. 4). Furthermore, even if overpressure builds up, the rate of increase may be too slow to be detected without monitoring over extended periods of time[171,185]. The rate of volumetric increase associated with flushing depends on the rate of fluid supply and thus may be faster than second boiling. On the other hand, the decrease of H_2O activity caused by the increase of CO_2 activity forces crystallisation, which increases magma viscosity and hinder the ability of magma to propagate to the surface and erupt[89].

To assess whether volatile exsolution can initiate magma chamber failure, we can compare the strain rate imposed to the wall rocks by exsolution $\dot{\gamma}_{ve}$ to the critical strain rate for reservoir failure, $\dot{\gamma}_{crit}$ (Eq. 4). If volatile exsolution is caused by flushing of CO_2-rich fluids from depth, $\dot{\gamma}_{ve}$ is function of the supply rate of CO_2[89] relative to the size and volatile

content of the resident magma chamber. If volatile exsolution is caused by crystallization and second boiling, $\dot{\gamma}_{ve}$ is linked to the cooling timescale of a magma reservoir[151]:

$$\dot{\gamma}_{cool} \sim \frac{1}{\tau_{cool}} \equiv \frac{\kappa}{V^{2/3}} \qquad (6)$$

where κ is the thermal diffusivity of the host crust. The faster a volatile-saturated magma cools, the faster volatiles exsolve and potentially pressurize a magma chamber. On the other hand, rapid cooling could lead to thermal death of a magma reservoir[102,136,151]. In Figure 4a we show an example of model results from Ref.[151], who consider the combined effects of magma recharge, crystallization and volatile exsolution, and viscoelastic behaviour of the crust. We frame their results in terms of the strain rates due to magma injection ($\dot{\gamma}_{in}$) and cooling/second boiling ($\dot{\gamma}_{cool}$) and how these compare to the critical strain rate for magma reservoir failure ($\dot{\gamma}_{crit}$) using a critical overpressure of ΔP_{crit} = 20 MPa and effective crust viscosity η_r of ~10^{19} Pa·s.

From the thermo-mechanical model of Ref.[151], we can compare the efficiency of magma recharge and second boiling as eruption triggers. When magma cooling dominates the strain rate ($\dot{\gamma}_{cool} > \dot{\gamma}_{in}$ and $\dot{\gamma}_{cool} > \dot{\gamma}_{crit}$), eruptions can be triggered by second boiling for volatile-saturated magmas. In addition, the fast cooling rate leads to a smaller number of eruptions that can occur before the magma reservoir freezes to some rheological lockup threshold[6]. This cooling-dominated regime would be favoured in smaller reservoirs subjected to lower recharge rates and embedded in relatively cold and more elastic crust (smaller $\dot{\gamma}_{crit}$). These conditions may prevail in immature systems that have not yet had the time and magma input to build up a large plumbing system in a warmer crust. Magma reservoirs that feed polygenetic volcanoes are likely already large enough that volatile exsolution is not an effective eruption trigger, or at least not as effective as magma injection. Using Laguna del Maule as an example, the size of the current subcaldera magma reservoir of ~30 km^3 implies $\dot{\gamma}_{cool}$~3 myr^{-1}, which is only fast enough to compete with $\dot{\gamma}_{crit}$ for the coldest/shallowest

range of crustal conditions (~6 km depth or less). When magma recharge dominates the strain rate ($\dot{\gamma}_{in} > \dot{\gamma}_{cool}$ and $\dot{\gamma}_{in} > \dot{\gamma}_{crit}$), many more eruptions can occur before the reservoir freezes (Fig. 4a), which suggests that eruptions are more likely triggered by magma recharge than second boiling. As of yet, we are not aware of natural systems that can definitively be categorized in the cooling- and exsolution-dominated regime. While this may partly be due to a bias of studies focused on larger and more active volcanoes, another hypothesis is that systems in the cooling regime are less likely to contribute to the volcanic record because they are short-lived.

As magma reservoirs grow, both the cooling- and recharge-induced strain rate decrease, the wall rocks become hotter and less viscous (BOX 1), and the compressibility of magma within the reservoir increases (Fig. 2). All together, these factors may eventually make eruptions more difficult to trigger, which implies that magma accumulation and reservoir growth is favoured in mature plumbing systems if they are still being fed by magma injections (Fig. 4).

3*. 2 External eruption triggers*

If a reservoir is already at pressure conditions close to those required for failure, small stress changes produced externally to the volcanic system may be sufficient to initiate magma ascent. As discussed in the previous section, under crustal conditions with deviatoric stress (from the lithostatic), fractures may not necessarily be purely tensile (Ref.[9]) so that shear strength can regulate the initiation of fractures. Crustal rocks usually have pre-existing cracks, so frictional strength is a lower limit for shear strength[186]. The summation of frictional strength and cohesion σ_0 is known as Coulomb failure stress

$$|\sigma| = \sigma_0 + f_s(\sigma_n - p_w) \qquad (7)$$

where σ_n is normal force acting on the fault surface, f_s is the friction coefficient.

External triggering mechanisms may act by changing the stress field and the strength of the host rock. Several phenomena can affect the strength: volcanic gas emissions associated with earthquakes may lubricate pre-existing cracks[187]; hot and acid volcanic gases sourced from magma may alter the host rocks around dikes, which lose strength[188,189] or are transformed in clay minerals that have lower friction coefficient[190,191]. Such modifications are important as even a reduction of the friction coefficient by 0.1 lowers the strength on the order of 1 MPa (Fig. 3). We thus consider that, in some cases, small external stress perturbations may reduce the strength of the surrounding rocks together with pore pressure[192].

.

3.2.1 Loading or unloading

A variety of surface loading processes can produce stress perturbations sufficient to trigger the release of magma from reservoirs at critical conditions. Climate change causes variations in the gravitational load of glaciers and ice sheets on land[193–196] and water masses at sea[197–199]. The correspondence between Milankovitch cycles and patterns of global volcanic activity suggests a link between climate change and volcanic eruptions[200]. Large-scale deglaciation can increase mantle melting at great depths (>50 km; Refs.[195,201,202]), while smaller-scale deglaciation can modulate lithospheric stress and promote dike formation[196,203,204]. Increased erosion associated with deglaciation can further enhance these effects[199]. Whether deglaciation encourages or discourages eruptions depends on the geometry of the surface load redistribution and the initial location and orientation of the dikes[205]. Similarly to glaciers, variations of surface loading associated with sea-level variations can also influence magma productivity[206–208].

The gravitational forces exerted by the sun and moon modulate stress in the Earth's crust on a variety of timescale from diurnal to seasonal, and although the stress perturbations associated with tides are small (~1 kPa), the hypothesis that tides can trigger eruptions dates

back almost a century[19,209–214]. Small stress perturbations could unclog pre-existing cracks and mobilise bubbles in a low-viscosity magma, thus modulating seismicity, outgassing, and potentially stimulating unrest[215,216]. Observations from persistently degassing volcanoes have shown an association especially between fortnight tides and degassing[217–220], although this correlation is not seen at every volcano[212,221], and even the same volcanic system may not show a consistent sensitivity to tides[215,222]. Additionally, the period of diurnal tides is close to that of daily fluctuation of atmospheric temperature and pressure, which for some volcanoes correlate with volcanic activity[223] and make the direct association between volcanic activity and tides less clear. However, for longer time scales, a statistically significant correlations is observed between seasonal variations of sea level and volcanic eruptions[224,225].

Volcanic activity itself can be a source of unloading. The climactic eruption of Mount St. Helens, 1980, was preceded by unloading of the summit area. A magma intrusion bulged the north flank causing its failure, which decompressed the shallow gaseous magma, triggering a laterally directed blast and Plinian column of volcanic ash[16,226–228]. Strength reduction of previously shattered dome rock due to crypto dome intrusion also might provoke collapse[229]. Similarly, a sector collapse event at Anak Krakatau volcano in 2018, which sourced a deadly tsunami, marked the onset of elevated volcanic activity, increased SO_2 emissions, and local earthquakes[17]. Degassing during quiescence can also cause unloading as the release of large amounts of gas from magma in the shallowest portions of the plumbing system may increase the pressure difference between the shallow and deep magma reservoirs triggering magma ascent from depth[230]. Such a top-down triggering mechanism is reflected by seismicity starting shallower than the estimated depth of the magma reservoir and migrating deeper[231].

3.2.2 Large earthquakes

Historically, some volcanoes have erupted after large earthquakes, and a causal relationship between earthquakes and eruptions was first proposed 50 years ago[232]. Statistical analysis shows a significant increase of the likelihood of eruption in a period of days to years following an earthquake[233,234]. Large eruptions rarely occur immediately after large earthquakes, but the sudden onset of volcanic unrest after the 1992 Landers earthquake at distances as great as 1200 km from the mainshock epicentre[235] renewed discussion on the mechanisms that might link earthquakes, volcanic unrest and eruptions[236]. Changes of volcanic monitoring parameters occurring immediately after large earthquakes are increasingly reported, including enhanced seismicity[237,238], deformation by dike intrusion[239,240] and subsidence[241,242]. Following earthquakes, volcanic degassing is enhanced in more mafic, open system volcanoes but tends to decrease in closed system volcanoes erupting more chemically evolved magmas[187]. This suggests that magma properties and the orientation of faults around a magma reservoir affect the response of volcanic systems to earthquakes[187,239,240,243]. Both volcano types including magma viscosity and characteristics of stress perturbation induced by earthquakes affect triggering efficiency[15]. The hydrothermal system is more sensitive to seismic triggering[15]. Importantly, not all volcanoes react to large earthquakes[244], suggesting that only volcanic systems that were already in a critical state react to earthquakes[234,245,246].

A fault rupture causes static and dynamic stress changes. The static stress is associated with permanent deformation of the crustal rock, and the dynamic stress change is caused by radiation of the seismic waves. Static stress quickly decays outside the near field[247], while dynamic stress further traveling as seismic waves[248,249]. These stress perturbations are small, but if the host rock is close to failure, they can help to initiate crack propagation by exceeding the Coulomb failure stress[250] (Eq. 7). Static stress change may modulate the permeability of the host rock, enhancing the magma ascent[251]. The surface

472 topography and its resonance can amplify the dynamic stress change[252]. Dynamic stress
473 change can force otherwise static bubbles to ascend and coalesce, resulting in shear
474 deformation, or sloshing[239,253–255]. The enhanced gas mobility could stimulate volcanic
475 activity in a variety of ways. High-temperature gas could change the friction coefficient along
476 open fractures surrounding the reservoir (Eq. 7)[256], and ease dike propagation. As an
477 example, the enhanced extrusion rate observed in the 2006 eruption of Merapi Volcano,
478 Indonesia, following the M_w 6.4 earthquake 50 km to the south[257,258], has interpreted to
479 results from the enhanced circulation in the crustal rocks of the CO_2 produced by the
480 decarbonation of the limestone bedrock[94,259,260].

481 While large distant earthquakes have been found to be weakly, but significantly
482 correlated with volcanic unrest and more rarely eruption, the effect of smaller local
483 earthquakes is less clear. As discussed later, propagating dikes often induce seismic swarms
484 whose cumulative seismic moment is correlated with the dike volume[261]. Thus, large dikes
485 may induce large earthquakes. The 2000 Miyakejima intrusion, for example, induced six
486 magnitude M >6 earthquakes (e.g. Ref.[262]). The seismicity induced by magma propagation
487 itself has been shown both on the base of observations and numerical models to tend to arrest
488 dikes, rather than promote their further propagation[23,263], and thus could contribute to prevent
489 an eruption. The same has been found for diffuse seismicity, as it relieves elastic energy and
490 increases the effective fracture toughness of rock, making it harder for dikes to reach the
491 surface[264]. Thus, local earthquakes may decrease or increase the likelihood of eruptions
492 depending on the specific case.

493 *3.2.3 Rainfall*

494 The strength of the host rock regulates gas and magma transport and depends on pore
495 pressure (Equations 1 and 7), suggesting that rainfall can plausibly influence volcanic

activities by changing the pore pressure. As an example, pore pressure perturbations of the order of 0.01-0.1 MPa can cause some earthquakes[265–267].

Indeed, enhanced volcanic activities after heavy rain have been reported for basaltic magma[268,269]. Eruption durations and explosivity at volcanoes such as Stromboli (Italy) has been observed to increase after rainstorms[270]. Additionally, the record-breaking levels of rainfall in early 2018 have been suggested to have facilitated the creation of a pathways for magma ascent of the 2018 rift eruption at Kilauea Volcano, which devastated the south-eastern part of the island[269,271]. Heavy rain events have also been suggested to have influenced seismicity rates at Mt. Merapi volcano[272] and Soufrière Hills Volcano, Montserrat[273], contributing to further destabilize their domes. Heavy rainfall also contributes to the hydrothermal pressurisation of domes[18], which has been deemed responsible for the collapses of domes at Soufrière Hills Volcano, Montserrat[274,275], Unzen, Japan[276], Merapi Volcano, Central Java, Indonesia[277], and Mount St. Helens[278] and for phreatic explosions[279]. The hydrothermal alteration also weakens the minerals to promote dome collapse[280]. Unloading by dome collapse decompresses the dome-core or shallow conduit lava, causing explosion and promoting further dome growth[275,281].

4. **Magma propagation to the surface**

Considering a scenario in which a reservoir containing eruptible magma has been pressurised to critical values, for an eruption to occur, magma has still to ascend for several kilometers before reaching the Earth's surface. In the following we will discuss the factors that can facilitate the ascent of magma to the surface and those that act to arrest magma propagation leading to an aborted eruption for both closed systems and frequently erupting volcanoes.

4.1 Magma ascent through conduits

Considering the presence of a previously established conduit to the surface, with no mechanical obstacles to eruption such as a plug of lava or layers of solid rock, the likelihood of the magma to erupt at the surface will be mostly determined by the properties of the magma. In particular the variations of viscosity and density upon ascent and decompression will determine the fate of the rising magma. Magma composition and initial volatile content will dictate the ascent dynamics, volume expansion and eruptive style (e.g., Ref.[282]). Parameters describing the host rock response to pressurization, such as conduit geometry, rock elastic parameters and coupling to a draining magma reservoir will contribute less to the decompression rate. Exceptions to this rationale are "thin", compressible conduit geometries: the thinner the conduit, the larger the role played by elasticity in regulating magma pressure (e.g., Ref.[283]). These dynamics have been described in many models that have progressed much in recent years and are now reaching the stage where they can be used to interpret quantitatively a variety of field observations such as the distribution of ejecta, lithic fragments, crustal deformation, and link them to conduit and magma parameters (e.g., Refs.[284,285]).

While many eruptions occur by magma flowing along pre-existing conduits, the lithostatic pressure increases with depth so that below ~1 km depth such conduits will rapidly collapse once drained. Moreover, even in "open conduit" volcanoes such as Etna or Stromboli the distribution of active vents changes dramatically over time scales of years or even months[286–288]. These considerations and observations demonstrate that the existence of pathways persistently used for degassing does not guarantee that magma will use them rather than opening new ones.

4.2 Magma propagation by diking: driving forces

What pathway magma will take to erupt is not only a central problem for hazard assessment[289], but also ultimately determines if magma will actually be able to reach the surface and erupt. The details of the path geometry, together with magma properties such as viscosity and density, dictate in many non-intuitive ways what could abort an eruption while magma is already on its way to the surface. Thus, the identification of the pathway the magma will take during ascent and the quantification of the stresses the magma pocket will experience are essential to determine if magma will eventually reach the surface.

Magma propagates through brittle rock by diking, a mechanism similar to hydraulic fracturing[8,9]. Dikes get arrested when the energy released during propagation is less than the energy required to create new fracture surface for the dike to advance[290], or, equivalently, when the stress intensity at their tip, K, becomes smaller than the rock's fracture toughness, K_c[291]. K is determined by the combined contribution of internal and external stresses or pressures and their variations along the dike plane, which is responsible for shaping the dike and its tip. Pressure is sometimes provided by hydraulic connection to a magma chamber, but dikes can also achieve enough pressure at their tip by being subject to "pressure gradients" (stress difference between dike tip and dike tail, over the length of the inflated region of the dike)[292]. That is because stresses may vary along the dike in a way to squeeze its tail and inflate its nose enough to achieve $K>K_c$, forcing dike propagation. This illustrates how the problem of "premature" dike arrest can be formulated in terms of dike size and the total stress gradient acting on the dike, that we indicate as $\Delta\gamma$. Both magma properties and external factors contribute to the total gradient $\Delta\gamma$ affecting a dike. One important such gradient originates from the difference between lithostatic and "magma-static" pressure along the dike, which varies as $\Delta\rho g \cos\theta$ (often called "buoyancy" pressure), where $\Delta\rho = \rho_r - \rho_m$ is the difference between host rock density, ρ_r, and magma density, ρ_m, g is the acceleration due to gravity, and θ is the dike's dip angle. In contrast, the viscous dissipation due to magma

570 flow tends to swell more the dike tail than its nose, and to slow down the dike. Additional
571 contributions need to be quantified case by case, and include stresses arising from uneven
572 overburden load distributions[293], differential stress accumulation linked to host rock
573 temperature gradients (e.g., Ref.[294]), regional stress gradients, previous intrusions and
574 earthquakes[289].
575
576 *4.3 Critical magma volumes for dike propagation*
577 Until recently, analytical equations for the 'critical volume for propagation', V_c, of
578 buoyancy-driven dikes filled with inviscid magma were only available in two
579 dimensions[295,296]. Ref.[28] extended the model to three dimensions considering only the
580 buoyancy gradient, but it is straightforward to rewrite the equation so to account for the total
581 stress gradient acting on the dike:
582 $$V_c = 0.75 \frac{(1-\nu)}{16\mu} \left(\frac{9\pi^4 K_c^8}{\Delta\gamma^5}\right)^{1/3} \quad (8)$$
583 where ν is Poisson's ratio, μ is shear modulus, K_c is the rock fracture toughness and $\Delta\gamma$ is the
584 total driving pressure gradient.
585 Since $V > V_c$ is required for a dike to carry on propagating, it follows that
586 propagation-hindering processes are those that either tend to decrease V, or, alternatively,
587 increase V_c (e.g. by increasing K_c or decreasing $\Delta\gamma$) during propagation. Dikes leave some
588 magma behind when they propagate because they cannot pinch perfectly closed at their back.
589 The higher the magma viscosity, the thicker their tail and the more abundant the magma left
590 on the way during propagation[8,22], which decreases the dike ability to move further.
591 Propagation-hindering processes that work by increasing K_c include seismicity, plasticity,
592 faulting[23,297] and approaching a more competent layer[298]. Factors contributing to decrease $\Delta\gamma$
593 include the increase of viscosity, resulting from decompression-induced crystallisation or
594 cooling[9], or a transition from vertical propagation to lateral when approaching a strong load

595 (e.g., Ref.[299]). The dike's dip angle θ is a rarely discussed, but important, factor for dike
596 arrest. A horizontal dike or sill (θ=0) will lack pressure due "buoyancy" and likely stall,
597 while shallow dipping dikes will require large volumes to propagate. Since uneven surface
598 loads have a large effect on the orientation of the principal stresses and thus on the dip of
599 dikes, a closer look at the shape of volcanic edifices will offer more clues on the chances of
600 dykes to reach the surface and feed an eruption. All this can be compensated, at least in part,
601 by other processes enhancing V, such as volatile exsolution and vesiculation or the dike
602 approaching the free surface[300].
603
604 *4.4 The pathway of dikes*
605 It is often assumed that magma is channeled by pre-existing weaknesses, such as
606 faults or fractures. However, the orientation of most faults is optimised for shear rather than
607 for opening[301], so that in most cases magma emplacement through faults requires more work
608 than opening a new path in a more convenient direction. This is why the vast majority of
609 dikes fail to occupy pre-existing faults and create their own pathways (e.g., Refs.[133,134,302]).
610 Seminal fieldwork and theoretical studies on the stress controls on dike propagation[124,130] has
611 shown that dikes tend to open perpendicular to the least compressive stress axis, σ_3. Such
612 "least resistance to opening" pathways are accurately determined by calculating the elastic
613 energy released during propagation[303–305]. Provided abundant magma pathways are observed
614 in an area, an accurate model of the stress field can be calibrated, allowing to forecast future
615 dike pathways[289]. Non-flat topography, heterogeneities of elastic parameters, land
616 movements, active faults, pressurized reservoirs, high pore pressure in hydrothermal systems,
617 previous intrusions may all contribute to stress heterogeneities and complex rotations of the
618 principal stresses[289,306]. Eruptive fissures' patterns on volcanoes are often attributed mainly to
619 stresses due to the pressurization of a magma reservoir of appropriate shape[126,307]). However,

620 Ref.[25] demonstrated that stresses from the growth of a volcanic edifice together with regional
621 stresses are often much larger than the stresses induced by pressurization of a magma
622 reservoir, and control the curvature of dikes in the field.

623 Many studies have confirmed that the shape of the volcanic edifice both exerts a
624 strong control on the orientation and dip of magma pathways and provides a driving force to
625 propagation, thereby controlling the time scales of magma migration and storage below the
626 volcanoes and the likelihood of dikes getting trapped or erupting.

627 Large volcanic edifices (stratocones and shield volcanoes) compress the underlying
628 rock, which results in both attracting dikes from offset magma reservoirs, and efficiently
629 trapping them at depth[264,299,303,304,308,309] (Fig. 5a); only dikes with a large buoyancy manage
630 to avert such trapping effect and erupt (e.g. Refs.[303,310]). If magma manages to intrude into the
631 edifice, topographic load gradients drive the dikes radially away from the summit[311–317] (Fig.
632 5b-c). The dikes may erupt or remain trapped due to the relation between magma density and
633 the density profile of the host rock[318,319], or by inducing graben faulting (e.g.. Refs.[130,263,320]).
634 The propagation is usually accompanied by seismicity, which can also trigger dike arrest by
635 releasing elastic energy[264].

636 Calderas are another example showing that the modulated stress field by topography
637 determines the direction, and influences the rate, of magma propagation (e.g., Ref.[289,321,322]).
638 Large-scale excavations such as a caldera cause a vertical σ_3 below the caldera floor, with
639 topographic load gradients from the caldera being surrounded by a rim trapping the dikes and
640 causing them to accumulate as stacked sills (e.g. Ref.[289,322]; Figs. 5d,e). Dikes may nucleate
641 as sub-horizontal intrusions and initially lack buoyancy, so that only large dikes may be able
642 to escape the stress trap. The gradual accumulation of caldera infill and growth of resurgent
643 domes may change the stress balance over the caldera cycle[323] and modify dike pathways and
644 vent patterns[289].

In summary, a magma propagation perspective on storage regions is that they represent a "bottleneck" where stresses slow down propagation or entirely trap the magma. If dikes achieve to escape from this trap, they still have great chances to get arrested on their way in a number of ways that can only be evaluated by combining concepts from petrology, structural geology and geophysics.

The issue with these concepts is that elastic stresses are notoriously very difficult to both measure directly and model (e.g., Ref.[324]). Elastic stresses result from many overlapping factors, some of which vary at the time scale of monitoring (e.g. magma reservoir stresses) and can be "sensed" through the deformation they are linked to, while others vary on much longer time scales (e.g. topographic loading) and "act in the background". In order to correctly model dike pathways we need to account for all stress-generating mechanisms, including both those that are linked to "visible" and "invisible" deformation, keeping in mind that "invisible" stresses might be the dominant ones, e.g. a 4-km-tall edifice generates ~100 MPa of compression on the underlying rock. The relative size of the individual contributions is challenging to estimate as they all depend on distinct poorly constrained factors such as the crustal profiles of rock density and rheology and various tectonic processes, to name just a few, and thus are difficult to bring together in a well-calibrated model. At the same time, magma trajectories are very sensitive to the ratios of the relative contributions[25,325], as such ratios determine the orientation of principal stress axes. This brings much confusion and uncertainty to stress models and has so far hindered accurate forecasting of dike paths[289,312,326].

5. **Summary and future perspectives**

One of the main goals of volcanology is to anticipate the future behaviour of volcanoes, an endeavour that requires a scientific understanding of the processes that lead to

the accumulation and transport of magma through the lithosphere, and the mechanisms that trigger eruptions. Physical models for magma reservoir assembly and growth demonstrate that the rate of magma supply to a reservoir is one of the key parameters that governs the rate of accumulation of eruptible magma, the pressurization of magma reservoirs required to initiate magma ascent to the surface, and the evolution of physical properties of both the magma and the surrounding crust (Fig.1). In general, the rate of eruptible magma accumulation in a reservoir increases with greater magma supply rates; however, greater magma supply rates can also pressurize and destabilize reservoirs, leading to heat and mass loss through magma withdrawal. As magma reservoirs grow, crystallizing magma becomes volatile saturated and host rocks become warmer and weaker (Fig.4). This changes the response of magma reservoirs to recharge, eruptions, and external perturbations such as earthquakes and changes in surface loading, leading to slower pressurization but larger volumes of magma withdrawal following reservoir failure. Similarly, the evolution of magma properties may impact the ability of magma to ascend through dikes. As magmas become more evolved and water-rich, the increased buoyancy could help to drive magmas to the surface; however, the increased viscosity could counteract these effects. In addition, structural changes to the volcano such as edifice growth or caldera collapse could alter the external stress field and hence the pathway of ascending dikes, in many cases trapping dikes in the shallow crust.

In light of the many factors that govern magma transport, storage, and eruption triggers, it becomes clear that in order to forecast future eruptions we need to be able to 1) characterize the current state of the magmatic system, including the distribution of magma volumes, pressure and temperature conditions, volatile content and saturation state; 2) characterize the “boundary conditions” that influence the magmatic system, such as the flux of magma from the mantle, and the rheology and stress field of the crust. Below we list the

695 major outstanding challenges to this endeavour that have emerged from our review, along
696 with some recommended avenues for future work to address these challenges.
697
698 1. The flux of primitive basaltic magmas from the mantle (and the proportion of
699 this flux that directly supplies crustal reservoirs) is perhaps the most
700 influential yet least constrained parameter that governs the growth and
701 evolution of crustal magmatic systems and the transport of magma to the
702 surface (Section 2.2, 3.1). Estimates based on eruptive volumes likely are
703 inaccurate unless the intrusive:extrusive ratio is well constrained; however, the
704 intrusive:extrusive ratio likely is not a fixed parameter but varies as a function
705 of magma supply rate, the size of the magma reservoir, and the thermal
706 maturity of the system.[11,12,36,100] Geodetic monitoring of recharge events
707 cannot uniquely constrain the mass of magma intruded[327], and the signal is
708 impacted by the presence of volatiles and viscoelastic response of the
709 crust[43,99]. Similarly, petrologic data, thermo-barometry and zircon
710 geochronology on erupted products provide snapshots of the magmatic
711 system, but only at discrete moments in time corresponding to past eruptions.
712 We suggest that although none of these datasets independently can constrain
713 the mantle flux and reservoir recharge rates, we can tighten our estimates
714 through the joint inversion of these data with numerical modeling of the
715 coupled thermal, mechanical, and chemical evolution of the plumbing system
716 (e.g., Refs.[36,75,284]).
717 2. The distribution of magma in the subsurface beneath volcanoes is key to
718 constraining the rate at which magma recharge can pressurize a reservoir
719 (Section 3) and places a lower bound on the potential size of an eruption, yet

our ability to "see" the magmatic system remains limited. The combination of data on eruptive volumes, co-eruptive deformation, and volatile content from melt inclusions may be used to place bounds on the size and depth of a reservoir feeding a particular eruption (e.g., Mount St. Helens 2004-2008[284]; Kīlauea Volcano 2018[328]), but this does not necessarily provide information about the distribution of magma throughout the rest of the crust, only the reservoir(s) being tapped by that eruption. Advances in seismic tomography, gravimetry, and magnetotellurics would be required to potentially resolve melt fractions at the resolutions needed to image melt-rich magma bodies[329].

3. Compared to their small abundance by mass, volatiles play an outsized role in both magma storage and transport by influencing magma properties such as compressibility, density, and viscosity; however, we are usually not able to directly measure the volatile content, saturation state, and distribution of volatiles in present-day reservoirs or during magma transport. In addition, the multiphase nature of volatile-saturated magmas makes it challenging to understand the dynamics of volatiles, melt, and crystals in a reservoir and their evolution over time, which has implications for both magma rheology (influencing viscosity and compressibility) and host-rock rheology (outgassing of hot, acid fluids can alter the strength and fracture distribution). More work to develop physical models of volatile behavior in reservoirs and to link these models to observations such as gas monitoring data may shed light on how volatiles migrate through reservoirs and how we might use monitoring data to constrain the current distribution of volatiles in subvolcanic reservoirs.
4. The pathway of magmatic dikes, which ultimately dictates the fate of magma ascending from depth, can be highly challenging to understand and anticipate.

745 Dike propagation is a complex multiphysics process for which numerical
746 models are still oversimplified. Dikes are also extremely sensitive to both
747 local- and regional-scale heterogeneities in crustal density and stress (e.g.,
748 Ref.[330]), which are usually only crudely characterized at most
749 volcanoes[289,293,310], as well as the distribution of internal magma pressure,
750 which evolves as a function of dike growth, connection to a reservoir, and
751 internal magmatic processes such as volatile exsolution which are rarely
752 considered in dike propagation models[331]. Dike propagation cannot be directly
753 observed in real time, but only indirectly through geophysical monitoring data
754 or geologic studies of eroded systems. Improvements to multiphysics models
755 for diking could come from engaging with other scientific communities (e.g.
756 engineers) who work on hydraulic fractures, but the application of these
757 models to dikes needs to integrate observations from the complementary
758 perspectives of geophysics and geology.

759 5. Once a magmatic system reaches a critical state, the timing of the eruption can
760 be modulated by external factors, such as earthquakes, dome collapses, tides,
761 and rainfall. Whether such mechanisms actually trigger an eruption depends
762 on both the magma conditions and the characteristics of the external force. In
763 the case of earthquakes, for instance, these could include the peak ground
764 velocity, frequency, and static stress change amplitude[15]. The strength of the
765 altered host rock also regulates the behavior of magma[332]. Accumulation of
766 such knowledge would help to anticipate eruptions. Another challenge in
767 understanding both internal and external eruption triggers is in establishing a
768 clear causal link; our confidence in identifying a particular trigger increases if
769 the triggering event occurs close to the volcano, produces a large change in

stress, and occurs immediately prior to the eruption (e.g., the landslide preceding the 1980 Mount St. Helens eruption[16]).

In summary, while we still need to understand many of the basic mechanisms and timescales involved in the storage and transport of magmas, the scientific community is making rapid progress. Simultaneously, new monitoring technology is being developed, instrumental networks are expanding, and global volcano databases are being established[30,46,333]. In order to take advantage of these developments to achieve effective eruption forecasting, we need to increase our efforts to reshape our theoretical understanding into forecast models. This requires merging simple (having a small number of independent parameters) deterministic physical models with data-driven approaches and statistical methods to help us estimate "in situ" rock and magma parameters that are crucial for determining how the system will evolve. Initiatives for independent model testing, which is standard practice in many fields, such as in seismic hazard analysis, may also help identifying the best strategies to move forward.

Figure Captions

Figure 1: Schematic illustration of a volcanic plumbing system with selected elements relevant for the assembly and trigger of volcanic eruptions. a) Fluids from the deepest portion of the crust. The panel shows how the chemistry of the degassed fluids at depth (expressed as H_2O and CO_2 molar fractions) change with magma cooling and crystallisation. b) Calibrated elemental map showing the distribution of anorthite content in plagioclase (left hand side) and aluminium (atoms per formula unit [apfu] – 23 oxygens) in clinopyroxene and amphibole (right hand side). The white rectangle shows selected crystals of plagioclase and amphibole with distinct chemical characteristics. These two groups of plagioclase and

795 amphiboles crystallised from magma of different chemical composition. c) illustration of the
796 potential evolution with time of the wall rock properties showing the increase of fracturing
797 and veins produced by hydrothermal activity. d) Chemistry of degassed fluids from a
798 subvolcanic reservoir exposed to the flushing of increasing amounts of CO_2.
799
800 **Figure 2: Relationships between temperature and magma properties and their temporal**
801 **evolution as calculated from thermal modelling.** The simulations were performed
802 considering the periodic input of magma in the crust (initial temperature 400 ^{o}C) at a depth
803 corresponding to a confining pressure of 200 MPa. The injected magma is a H_2O-saturated
804 (CO_2-free) andesite, with temperature-melt fraction determined experimentally by Ref.[334].
805 The volume of excess fluids is calculated assuming full incompatibility in the crystallising
806 minerals and ideal behaviour. Magma compressibility was calculated following Ref.[100] at
807 pressure of 200 MPa and considering an overpressure of 1MPa (the results are virtually
808 identical for overpressures of 10 MPa). We consider that excess fluids leave the system once
809 magma cools to solidus temperature. a) Variation of melt and excess fluid fraction, and
810 compressibility as function of temperature. b, c) Total volume of injected magma (black line),
811 reservoir (blue line) and eruptible magma (red line) as function of time for two rates of
812 magma input in the crust (expressed as vertical accretion rates). The coloured curves shows
813 spikes corresponding to the injection of a new sill into the system, while the black line is
814 smooth because it is calculated using the average rate of magma input. d, e) Average crystal
815 fraction, eruptible/injected magma volume and compressibility as function of time calculate
816 from the thermal modelling results presented in panel b and c, respectively.
817
818 **Box 1: Schematic illustration reporting physical properties of magma[335] and wall**
819 **rock[9,141,150] relevant for the pressurization of magma reservoirs.** Processes leading to

variation of volume (ΔV), such as magma injection or volatile exsolution, can lead to the pressurisation of the reservoir. The host rock surrounding the magma chamber can behave both viscously and elastically. When strain rate produced by magma supply or volatile exsolution is sufficiently slow, the host rock deforms viscously, which may inhibit nucleation and propagation of a crack in the wall rock. In contrast, at high strain rates the wall rock behave elastically and overpressure increases in the magma reservoir until it exceeds a critical value for failure and cracks propagate into the wall rock, initiating magma transport. Typical magma input rates $\dot{V}_{in}$ vary between 10^{-4} and 10^{-2} km^3/year (Refs.[336,337]). Considering volume of spherical magma reservoir (V) between 1 and 100 km^3, the range of strain rate produced by such rates of magma input can be calculated as $\dot{\gamma}_{in} = \frac{\dot{V}_{in}}{V} = 10^{-15} - 10^{-9} s^{-1}$ or 0.03 – 30,000 myr^{-1}.

Figure 3: A summary of stress and pressure scales. Continuous blue and pink curves show the stress required for viscous deformation of wet quartz and wet plagioclase at a shear rate of $2.5x10^{-12}$ s^{-1} calculated by Equation 1 (Refs.[338,339]). This shear rate corresponds to a magma supply of 0.001 km^3/year into a magma chamber with a radius of 1km. We also calculated the required stress to deform quartz at other strain rates, as shown in the legend. We consider a temperature gradient of 30 ^oC/km with a surface temperature of 20 ^oC. The thick blue curve refers to a temperature of 500 ^oC higher than the geotherm and shows the effect of temperature increase of the wall rock due to the presence of magma in the crust. Red and black-gray curves provide the dry tensile failure condition and friction strength without cohesion calculated by Equations 1 and 7, respectively, where f_s is friction coefficient. The boxes of earthquake, rain, the arrow with the note of landslide and degassing, purple region labelled glacier/sea level, and the green-dashed line labelled tide indicates the range of stress perturbations caused by each respective phenomenon.

845

846 **Figure 4: a)** Regime diagram of the number of diking events ("eruptions") from a magma
847 chamber before the chamber freezes to 50% crystal volume fraction, based on the model of
848 Degruyter and Huber (2014). Number of eruptions is shown as a function of the strain rates
849 due to magma injection $\dot{\gamma}_{in}$, cooling and volatile exsolution $\dot{\gamma}_{cool}$, and the critical strain rate
850 for diking to occur $\dot{\gamma}_{crit}$. In the upper left region, eruptions are triggered by second boiling. In
851 the upper right region, eruptions are triggered by magma injection. In the lower third of the
852 diagram, no eruptions occur because the critical strain rate is not met. Contours of number of
853 eruptions are shown by the coloured lines. The six triangles are examples of where systems
854 would plot in regime space for the hypothetical conditions shown in panel (b). **b)**
855 Hypothetical values for magma chamber volumes, crust viscosity and magma injection rates
856 over time. Initially we imagine a small chamber in a cold, higher-viscosity crust. As magma
857 injection rates increase, the crust warms up and viscosity drops, and eventually the magma
858 chamber grows to larger sizes. In the last example (triangle 6), magma injection wanes, the
859 crust starts to cool again (viscosity increases) and the chamber loses volume as it freezes.
860

861 **Figure 5**: Shallow pathways of dikes from the geological record and fluid injection
862 experiments in gelatine. **a)** Gravitational loading attracts and focuses deep dikes, before
863 causing their arrest at depth (from Ref.[308], with permission). **b)** Gravitational loading causes
864 dikes within a stratocone or shield volcano to propagate radially away from the centre of the
865 edifice. Red bodies are injected dyed water, the yellow mass is solidified gelatine shaped to
866 model a gravitationally loaded volcanic edifice. Unpublished experiment**. c)** Map of Summer
867 Coon volcanic center, showing radial dykes as black segments. From Ref.[340], with
868 permission. **d)** Three-dimensional model of cone-sheets (blue ribbons) at the Ardnamurchan
869 igneous complex projected on the basis of their surface expression. From Ref.[341], with

permission. **e)** Asymmetric excavation simulating a caldera or rift system. The black curves are pathways of injected dyed water. Unpublished experiment.

REFERENCES

1. Cañón-Tapia, E. Volcanic eruption triggers: A hierarchical classification. *Earth-Science Rev.* **129**, 100–119 (2014).
2. Parfitt, E. A. & Wilson, L. *Fundamentals of physical volcanology*. (Blackwell Publishing Ltd, 2008).
3. Manga, M. *et al. Volcanic eruptions and their repose, unrest, precursors, and timing*. *Volcanic Eruptions and Their Repose, Unrest, Precursors, and Timing* (2017). doi:10.17226/24650.
4. Taisne, B., Tait, S. & Jaupart, C. Conditions for the arrest of a vertical propagating dyke. *Bull. Volcanol.* **73**, 191–204 (2011).
5. Caricchi, L. *et al.* Non-Newtonian rheology of crystal-bearing magmas and implications for magma ascent dynamics. *Earth Planet. Sci. Lett.* **264**, 402–419 (2007).
6. Lejeune, A. M. & Richet, P. Rheology of Crystal-Bearing Silicate Melts - an Experimental-Study at High Viscosities. *J. Geophys. Res. Earth* **100**, 4215–4229 (1995).
7. Marsh, B. D. On the Crystallinity, Probability of Occurrence, and Rheology of Lava and Magma. *Contrib. to Mineral. Petrol.* **78**, 85–98 (1981).
8. Rivalta, E., Taisne, B., Bunger, A. P. & Katz, R. F. A review of mechanical models of dike propagation: Schools of thought, results and future directions. *Tectonophysics* **638**, 1–42 (2015).
9. Rubin, A. M. Propagation of magma-filled cracks. *Annu. Rev. Earth Planet. Sci.*

(1995).

10. Takeuchi, S. Preeruptive magma viscosity: An important measure of magma eruptibility. *J. Geophys. Res.* **116**, B10201 (2011).

11. Annen, C. From plutons to magma chambers: Thermal constraints on the accumulation of eruptible silicic magma in the upper crust. *Earth Planet. Sci. Lett.* **284**, 409–416 (2009).

12. Karakas, O., Degruyter, W., Bachmann, O. & Dufek, J. Lifetime and size of shallow magma bodies controlled by crustal-scale magmatism. *Nat. Geosci.* **310**, 511 (2017).

13. Grosfils, E. B. Magma reservoir failure on the terrestrial planets: Assessing the importance of gravitational loading in simple elastic models. *J. Volcanol. Geotherm. Res.* **166**, 47–75 (2007).

14. Gudmundsson, A. Magma chambers: Formation, local stresses, excess pressures, and compartments. *J. Volcanol. Geotherm. Res.* **237**–**238**, 19–41 (2012).

15. Seropian, G., Kennedy, B., Walter, T., Ichihara, M. & Jolly, A. A review framework of how earthquakes trigger volcanic eruptions. *Nat. Commun.* **12**, 1–13 (2021).

16. Lipman, P. W. & Mullineaux, D. R. *The 1980 eruptions of Mount St. Helens, Washington*. vol. 1250 (U.S. Geol. Surv. Prof. Pap., 1981).

17. Walter, T. R. *et al.* Complex hazard cascade culminating in the Anak Krakatau sector collapse. *Nat. Commun.* (2019) doi:10.1038/s41467-019-12284-5.

18. Elsworth, D., Voight, B., Thompson, G. & Young, S. R. Thermal-hydrologic mechanism for rainfall-triggered collapse of lava domes. *Geology* **32**, 969–972 (2004).

19. Sparks, R. S. J. Triggering of volcanic eruptions by Earth tides. *Nature* **290**, 448 (1981).

20. Blundy, J. & Cashman, K. Ascent-driven crystallisation of dacite magmas at Mount St Helens, 1980-1986. *Contrib. to Mineral. Petrol.* **140**, 631–650 (2001).

21. La Spina, G., Burton, M., de rsquo Michieli Vitturi, M. & Arzilli, F. Role of syn-eruptive plagioclase disequilibrium crystallization in basaltic magma ascent dynamics. *Nat. Commun.* **7**, 1–10 (2016).

22. Rubin, A. M. Getting Granite Dikes Out of the Source Region. *J. Geophys. Res. Earth* **100**, 5911–5929 (1995).

23. Maccaferri, F., Rivalta, E., Passarelli, L. & Aoki, Y. On the mechanisms governing dike arrest: Insight from the 2000 Miyakejima dike injection. *Earth Planet. Sci. Lett.* (2016).

24. Pinel, V. & Jaupart, C. The effect of edifice load on magma ascent beneath a volcano. *Philos. Trans. R. Soc. London. Ser. A, Math. Phys. Sci.* **358**, 1515–1532 (2000).

25. Roman, A. & Jaupart, C. The impact of a volcanic edifice on intrusive and eruptive activity. *Earth Planet. Sci. Lett.* **408**, 1–8 (2014).

26. Taisne, B. & Tait, S. Effect of solidification on a propagating dike. *J. Geophys. Res.* **116**, B01206 (2011).

27. Townsend, M. & Huber, C. A critical magma chamber size for volcanic eruptions. *Geology* **48**, 431–435 (2020).

28. Davis, T. Critical Fluid Injection Volumes for Uncontrolled Fracture Ascent Geophysical Research Letters. **v**, (2020).

29. Moran, S. C., Newhall, C. & Roman, D. C. Failed magmatic eruptions: Late-stage cessation of magma ascent. *Bull. Volcanol.* **73**, (2011).

30. Venzke, E. (Ed). Global Volcanism Program | Volcanoes of the World (VOTW) Database Information. *Smithsonian Institution* (2013).

31. Annen, C., Blundy, J. D., Leuthold, J. & Sparks, R. S. J. Construction and evolution of igneous bodies: Towards an integrated perspective of crustal magmatism. *Lithos* **230**, 206–221 (2015).

945 32. Crisp, J. A. Rates of Magma Emplacement and Volcanic Output. *J. Volcanol.*
946 *Geotherm. Res.* **20**, 177–211 (1984).
947 33. Jicha, B. R. & Jagoutz, O. Magma Production Rates for Intraoceanic Arcs. *Elements*
948 **11**, 105–111 (2015).
949 34. Weber, G., Caricchi, L., Arce, J. L. & Schmitt, A. K. Determining the current size and
950 state of subvolcanic magma reservoirs. *Nat. Commun.* (2020) doi:10.1038/s41467-020-
951 19084-2.
952 35. White, S. M., Crisp, J. A. & Spera, F. J. Long-term volumetric eruption rates and
953 magma budgets. *Geochemistry Geophys. Geosystems* **7**, Q03010 (2006).
954 36. Weber, G., Simpson, G. & Caricchi, L. Magma diversity reflects recharge regime and
955 thermal structure of the crust. *Sci. Rep.* **10**, 11867 (2020).
956 37. Aiuppa, A., Fischer, T. P., Plank, T. & Bani, P. CO2 flux emissions from the Earth's
957 most actively degassing volcanoes, 2005–2015. *Sci. Rep.* **9**, 2005–2015 (2019).
958 38. Biggs, J. & Pritchard, M. E. Global Volcano Monitoring: What Does It Mean When
959 Volcanoes Deform? *Elements* (2017).
960 39. Burton, M., Allard, P., Muré, F. & La Spina, A. Magmatic gas composition reveals the
961 source depth of slug-driven Strombolian explosive activity. *Science (80-.).* **317**, 227–
962 230 (2007).
963 40. Carn, S. A., Fioletov, V. E., McLinden, C. A., Li, C. & Krotkov, N. A. A decade of
964 global volcanic SO2 emissions measured from space. *Sci. Rep.* 1–12 (2017).
965 41. Furtney, M. A. *et al.* Synthesizing multi-sensor, multi-satellite, multi-decadal datasets
966 for global volcano monitoring. *J. Volcanol. Geotherm. Res.* **365**, 38–56 (2018).
967 42. Ganci, G., Vicari, A., Fortuna, L. & del Negro, C. The HOTSAT volcano monitoring
968 system based on combined use of SEVIRI and MODIS multispectral data. *Ann.*
969 *Geophys.* **54**, 544–550 (2011).

43. Kilbride, B. M., Edmonds, M. & Biggs, J. Observing eruptions of gas-rich compressible magmas from space. *Nat. Commun.* **7**, 13744 (2016).
44. Reath, K. *et al.* Thermal, Deformation, and Degassing Remote Sensing Time Series (CE 2000–2017) at the 47 most Active Volcanoes in Latin America: Implications for Volcanic Systems. *J. Geophys. Res. Solid Earth* **124**, (2019).
45. Ripepe, M., Harris, A., Geothermal, R. C.-J. of V. and & 2002, undefined. Thermal, seismic and infrasonic evidences of variable degassing rates at Stromboli volcano. *Elsevier*.
46. Costa, F. *et al.* WOVOdat – the global volcano unrest database aimed at improving eruption forecasts. *Disaster Prev. Manag. An Int. J.* **28**, 738–751 (2019).
47. Dempsey, D. E., Cronin, S. J., Mei, S. & Kempa-Liehr, A. W. Automatic precursor recognition and real-time forecasting of sudden explosive volcanic eruptions at Whakaari, New Zealand. *Nat. Commun.* **11**, 1–8 (2020).
48. Ebmeier, S. K., Biggs, J., Mather, T. A. & Amelung, F. On the lack of InSAR observations of magmatic deformation at Central American volcanoes. *J. Geophys. Res. Solid Earth* **118**, 2571–2585 (2013).
49. Phillipson, G., Sobradelo, R. & Gottsmann, J. Global volcanic unrest in the 21st century: An analysis of the first decade. *J. Volcanol. Geotherm. Res.* **264**, 183–196 (2013).
50. Sheldrake, T. E., Sparks, R. S. J., Cashman, V. K., Wadge, G. & Aspinall, W. P. Similarities and differences in the historical records of lava dome-building volcanoes: Implications for understanding magmatic processes and eruption forecasting. *Earth-Science Rev.* **160**, 240–263 (2016).
51. Cashman, V. K. & Marsh, B. D. Crystal size distribution (CSD) in rocks and the kinetics and dynamics of crystallization II: Makaopuhi lava lake. *Contrib. to Mineral.*

995 *Petrol.* **99**, 292–305 (1988).
996 52. Li, W. & Costa, F. A thermodynamic model for F-Cl-OH partitioning between silicate
997 melts and apatite including non-ideal mixing with application to constraining melt
998 volatile budgets. *Geochim. Cosmochim. Acta* **269**, 203–222 (2020).
999 53. Hammer, J. E. Experimental studies of the kinetics and energetics of magma
1000 crystallization. *Rev. Mineral. Geochemistry* **69**, 9–59 (2008).
1001 54. Martel, C. *et al.* Experimental Simulations of Magma Storage and Ascent. in *Advances*
1002 *in Volcanology* vol. 69 101–110 (Springer Berlin Heidelberg, 2017).
1003 55. Mollo, S., Blundy, J. D., Iezzi, G., Scarlato, P. & Langone, A. The partitioning of trace
1004 elements between clinopyroxene and trachybasaltic melt during rapid cooling and
1005 crystal growth. *Contrib. to Mineral. Petrol.* **166**, 1633–1654 (2013).
1006 56. Nandedkar, R. H., Ulmer, P. & Müntener, O. Fractional crystallization of primitive,
1007 hydrous arc magmas: an experimental study at 0.7GPa. *Contrib. to Mineral. Petrol.*
1008 **167**, 1015 (2014).
1009 57. Putirka, K. D. Introduction to Minerals, Inclusions and Volcanic Processes. *Rev.*
1010 *Mineral. Geochemistry* **69**, 1–8 (2008).
1011 58. Riker, J. M., Blundy, J. D., Rust, A. C., Botcharnikov, R. E. & Humphreys, M. C. S.
1012 Experimental phase equilibria of a Mount St. Helens rhyodacite: a framework for
1013 interpreting crystallization paths in degassing silicic magmas. *Contrib. to Mineral.*
1014 *Petrol.* 1–22 (2015).
1015 59. Scaillet, B. & Evans, B. W. The 15 June 1991 eruption of Mount Pinatubo. I. Phase
1016 equilibria and pre-eruption P-T-fO(2)-fH(2)O conditions of the dacite magma. *J.*
1017 *Petrol.* **40**, 381–411 (1999).
1018 60. Kahl, M. *et al.* Compositionally zoned crystals and real-time degassing data reveal
1019 changes in magma transfer dynamics during the 2006 summit eruptive episodes of Mt.

Etna. *Bull. Volcanol.* **75**, 1114–1115 (2013).

61. Melnik, O. E., Blundy, J. D., Rust, A. C. & Muir, D. Subvolcanic plumbing systems imaged through crystal size distributions. *Geology* (2011).

62. Moretti, R., Arienzo, I., Civetta, L., Orsi, G. & Papale, P. Multiple magma degassing sources at an explosive volcano. *Earth Planet. Sci. Lett.* **367**, 95–104 (2013).

63. Mutch, E. J. F., Maclennan, J., Shorttle, O., Edmonds, M. & Rudge, J. F. Rapid transcrustal magma movement under Iceland. *Nat. Geosci.* **12**, 569–574 (2019).

64. Myers, M. L., Wallace, P. J., Wilson, C. J. N., Morter, B. K. & Swallow, E. J. Prolonged ascent and episodic venting of discrete magma batches at the onset of the Huckleberry Ridge supereruption, Yellowstone. *Earth Planet. Sci. Lett.* **451**, 285–297 (2016).

65. Neal, C. A. *et al.* The 2018 rift eruption and summit collapse of Kīlauea Volcano. *Science (80-.).* **59**, eaav7046–14 (2018).

66. Neave, D. A. & Maclennan, J. Clinopyroxene Dissolution Records Rapid Magma Ascent. *Front. Earth Sci.* **8**, 188 (2020).

67. Pallister, J. S., Hoblitt, R. P. & Reyes, A. G. A basalt trigger for the 1991 eruptions of Pinatubo volcano? *Nature* **356**, 426–428 (1992).

68. Pistolesi, M., Donne, D. D., Pioli, L., Rosi, M. & Ripepe, M. The 15 March 2007 explosive crisis at Stromboli volcano, Italy: Assessing physical parameters through a multidisciplinary approach. *J. Geophys. Res. Solid Earth* **116**, 1–18 (2011).

69. Sheldrake, T. Long-term forecasting of eruption hazards: A hierarchical approach to merge analogous eruptive histories . *J. Volcanol. Geotherm. Res.* **286**, 15–23 (2014).

70. Paulatto, M. *et al.* Magma chamber properties from integrated seismic tomography and thermal modeling at Montserrat. *Geochemistry Geophys. Geosystems* **13**, Q01014 (2012).

71. Stock, M. J., Humphreys, M. C. S., Smith, V. C., Isaia, R. & Pyle, D. M. Late-stage volatile saturation as a potential trigger for explosive volcanic eruptions. *Nat. Geosci.* **9**, 249–254 (2016).

72. Thomas, M. E. & Neuberg, J. What makes a volcano tick–A first explanation of deep multiple seismic sources in ascending magma. *Geology* **40**, 351–354 (2012).

73. Wieser, P. E., Edmonds, M., Maclennan, J. & Wheeler, J. Microstructural constraints on magmatic mushes under Kīlauea Volcano, Hawai'i. *Nat. Commun.* **11**, (2020).

74. Aiuppa, A. *et al.* A model of degassing for Stromboli volcano. *Earth Planet. Sci. Lett.* **295**, 195–204 (2010).

75. Anderson, K. R. & Poland, M. P. Bayesian estimation of magma supply, storage, and eruption rates using a multiphysical volcano model: Kilauea Volcano, 2000-2012. *Earth Planet. Sci. Lett.* **447**, 161–171 (2016).

76. Saunders, K., Blundy, J., Dohmen, R. & Cashman, V. K. Linking Petrology and Seismology at an Active Volcano. *Science (80-.).* **336**, 1023–1027 (2012).

77. Curry, A., Caricchi, L. & Lipman, P. W. Magmatic evolution of zoned and unzoned ignimbrites: evidence from four rapid-sequence, caldera-forming eruptions in the San Juan Mountains, Colorado. *J. Petrol.* **in review**, (2020).

78. Caricchi, L., Biggs, J., Annen, C. & Ebmeier, S. The influence of cooling , crystallisation and re-melting on the interpretation of geodetic signals in volcanic systems. *Earth Planet. Sci. Lett.* **388**, 166–174 (2014).

79. Trasatti, E. *et al.* Magma Degassing as a Source of Long-Term Seismicity at Volcanoes: The Ischia Island (Italy) Case. *Geophys. Res. Lett.* **46**, 14421–14429 (2019).

80. Borisova, A. Y. *et al.* H2O-CO2-S fluid triggering the 1991 Mount Pinatubo climactic eruption (Philippines). *Bull. Volcanol.* **76**, 1–9 (2014).

81. Till, C. B. *et al.* The causes of spatiotemporal variations in erupted fluxes and compositions along a volcanic arc. *Nat. Commun.* **10**, (2019).
82. Cheng, L. & Costa, F. Statistical analysis of crystal populations and links to volcano deformation for more robust estimates of magma replenishment volumes. *Geology* **47**, 1171–1175 (2019).
83. Chiodini, G. *et al.* Magmas near the critical degassing pressure drive volcanic unrest towards a critical state. *Nat. Commun.* **7**, 1–9 (2016).
84. Christopher, T., Edmonds, M., Humphreys, M. C. S. & Herd, R. A. Volcanic gas emissions from Soufrière Hills Volcano, Montserrat 1995-2009, with implications for mafic magma supply and degassing. *Geophys. Res. Lett.* **37**, n/a—n/a (2010).
85. Edmonds, M. *et al.* Excess volatiles supplied by mingling of mafic magma at an andesite arc volcano. *Geochemistry Geophys. Geosystems* **11**, (2010).
86. Humphreys, M. C. S. *et al.* A new method to quantify the real supply of mafic components to a hybrid andesite. *Contrib. to Mineral. Petrol.* **165**, 191–215 (2012).
87. Kent, A. J. R., Darr, C., Koleszar, A. M., Salisbury, M. J. & Cooper, K. M. Preferential eruption of andesitic magmas through recharge filtering. *Nat. Geosci.* **3**, 631–636 (2010).
88. Papale, P., Moretti, R. & Barbato, D. The compositional dependence of the saturation surface of H 2 O+ CO 2 fluids in silicate melts. *Chem. Geol.* **229**, 78–95 (2006).
89. Caricchi, L., Sheldrake, T. E. & Blundy, J. Modulation of magmatic processes by CO2 flushing. *Earth Planet. Sci. Lett.* **491**, 160–171 (2018).
90. Yoshimura, S. & Nakamura, M. Carbon dioxide transport in crustal magmatic systems. *Earth Planet. Sci. Lett.* **307**, 470–478 (2011).
91. Spilliaert, N., Allard, P., Métrich, N. & Sobolev, A. V. Melt inclusion record of the conditions of ascent, degassing, and extrusion of volatile-rich alkali basalt during the

powerful 2002 flank eruption of Mount Etna (Italy). *J. Geophys. Res. Solid Earth* **111**, (2006).

92. Bachmann, O. & Bergantz, G. W. Gas percolation in upper-crustal silicic crystal mushes as a mechanism for upward heat advection and rejuvenation of near-solidus magma bodies. *J. Volcanol. Geotherm. Res.* **149**, (2006).

93. Blundy, J., Cashman, V. K., Rust, A. & Witham, F. A case for CO2-rich arc magmas. *Earth Planet. Sci. Lett.* **290**, 289–301 (2010).

94. Deegan, F. M. *et al.* Magma-Carbonate Interaction Processes and Associated CO2 Release at Merapi Volcano, Indonesia: Insights from Experimental Petrology. *J. Petrol.* **51**, 1027–1051 (2010).

95. Coleman, D. S., Bartley, J. M., Glazner, A. F. & Pardue, M. J. Is chemical zonation in plutonic rocks driven by changes in source magma composition or shallow-crustal differentiation? *Geosphere* **8**, 1568 (2012).

96. de Saint-Blanquat, M. *et al.* Multiscale magmatic cyclicity, duration of pluton construction, and the paradoxical relationship between tectonism and plutonism in continental arcs. *Tectonophysics* **500**, 20–33 (2011).

97. Glazner, A. F., Bartley, J. M., Coleman, D. S., Gray, W. & Taylor, R. Z. Are plutons assembled over millions of years by amalgamation from small magma chambers? *GSA TODAY* **14**, 4–11 (2004).

98. Annen, C., Blundy, J. D. & Sparks, R. S. J. The genesis of intermediate and silicic magmas in deep crustal hot zones. *J. Petrol.* **47**, 505–539 (2006).

99. Edmonds, M. & Woods, A. W. Exsolved volatiles in magma reservoirs. *J. Volcanol. Geotherm. Res.* **368**, 13–30 (2018).

100. Townsend, M., Huber, C., Degruyter, W. & Bachmann, O. Magma Chamber Growth During Intercaldera Periods: Insights From Thermo-Mechanical Modeling With

Applications to Laguna del Maule, Campi Flegrei, Santorini, and Aso. *Geochemistry Geophys. Geosystems* 18–63 (2019).

101. Caricchi, L. & Blundy, J. Experimental petrology of monotonous intermediate magmas. *Geol. Soc. London, Spec. Publ.* **422**, 105–130 (2015).

102. Jellinek, A. M. & DePaolo, D. J. A model for the origin of large silicic magma chambers: precursors of caldera-forming eruptions. *Bull. Volcanol.* **65**, 363–381 (2003).

103. Caricchi, L., Annen, C., Blundy, J., Simpson, G. & Pinel, V. Frequency and magnitude of volcanic eruptions controlled by magma injection and buoyancy. *Nat. Geosci.* **7**, 126–130 (2014).

104. Malfait, W. J. *et al.* Supervolcano eruptions driven by melt buoyancy in large silicic magma chambers. *Nat. Geosci.* **7**, 122–125 (2014).

105. Parmigiani, A., Degruyter, W., Leclaire, S., Huber, C. & Bachmann, O. The mechanics of shallow magma reservoir outgassing. *Geochemistry, Geophys. Geosystems* **18**, (2017).

106. Mittal, T. & Richards, M. A. Volatile Degassing From Magma Chambers as a Control on Volcanic Eruptions. *J. Geophys. Res. Solid Earth* **124**, (2019).

107. Degruyter, W., Parmigiani, A., Huber, C. & Bachmann, O. How do volatiles escape their shallow magmatic hearth? *Philos. Trans. R. Soc. A Math. Phys. Eng. Sci.* **377**, (2019).

108. Jellinek, A. M. & Kerr, R. C. *Mixing and compositional stratification produced by natural convection: 2. Applications to the differentiation of basaltic and silicic magma chambers and komatiite lava flows*. *JOURNAL OF GEOPHYSICAL RESEARCH* vol. 104 https://agupubs.onlinelibrary.wiley.com/doi/abs/10.1029/1998JB900117 (1999).

109. Huber, C., Bachmann, O., Letters, M. M.-E. and P. S. & 2009, undefined.

Homogenization processes in silicic magma chambers by stirring and mushification (latent heat buffering). *Elsevier*.

110. Burgisser, A., Nature, G. B.- & 2011, undefined. A rapid mechanism to remobilize and homogenize highly crystalline magma bodies. *nature.com*.

111. Sparks, S. R. J., Sigurdsson, H. & Wilson, L. Magma mixing: A mechanism for triggering acid explosive eruptions. *Nature* **267**, 315–318 (1977).

112. Degruyter, W., Huber, C., Bachmann, O., Cooper, K. M. & Kent, A. J. R. Influence of Exsolved Volatiles on Reheating Silicic Magmas by Recharge and Consequences for Eruptive Style at Volc an Quizapu (Chile). *Wiley Online Libr.* **18**, 4123–4135 (2017).

113. Nature, J. E.- & 1980, undefined. *Vesiculation of mafic magma during replenishment of silicic magma reservoirs*. *nature.com* https://idp.nature.com/authorize/casa?redirect_uri=https://www.nature.com/articles/288446a0&casa_token=XU1Op0Ow7wAAAAAA:zoO_H_COTSQEbP8NT-bnaP3gGJ7kXI0pUXzcHRJhOwqy8ZE1NtkttqyCopwwtLZ5YzPOFG4kP2ulRxbZ1Q (1980).

114. Huppert, H. E., Stephen, R., Sparkst, J. & Turner, J. S. *Effects of volatiles on mixing in calc-alkaline magma systems*. *Nature* vol. 297 https://idp.nature.com/authorize/casa?redirect_uri=https://www.nature.com/articles/297554a0&casa_token=UEwdnF5_NvMAAAAA:P13ExsugraSxsAvpcdLGXq2soUrRR7PJJ-iDIKTz9-HlcxeU8muLvVGICbGgVmR5BE9Tp6d-8ppFTkD3_A (1982).

115. Ruprecht, P. *et al.* Modeling of gas-driven magmatic overturn: Tracking of phenocryst dispersal and gathering during magma mixing Geochemistry Geophysics Geosystems Geochemistry Geophysics Geosystems. *Wiley Online Libr.* **9**, (2008).

116. Phillips, J., Letters, A. W.-E. and P. S. & 2002, undefined. Suppression of large-scale magma mixing by melt–volatile separation. *Elsevier*.

117. Huber, C. & Parmigiani, A. A Physical Model for Three-Phase Compaction in Silicic Magma Reservoirs. *J. Geophys. Res. Solid Earth* **123**, 2685–2705 (2018).

118. Murphy, M. D. *et al. The role of magma mixing in triggering the current eruption at the Soufriere Hills volcano, Montserrat, West Indies*. *Wiley Online Library* vol. 25 https://agupubs.onlinelibrary.wiley.com/doi/abs/10.1029/98GL00713 (1998).

119. Letters, D. S.-E. and P. S. & 2000, undefined. Thermal effects of the intrusion of basaltic magma into a more silicic magma chamber and implications for eruption triggering. *Elsevier*.

120. Bain, A. A., Jellinek, A. M. & Wiebe, R. A. Quantitative field constraints on the dynamics of silicic magma chamber rejuvenation and overturn. *Contrib. to Mineral. Petrol.* **165**, 1275–1294 (2013).

121. Walker, G. P. L. Koolau Dike Complex, Oahu: Intensity and origin of a sheeted-dike complex high in a Hawaiian volcanic edifice. *Geology* **14**, 310–313 (1986).

122. Gudmundsson, A. Emplacement of dikes , sills and crustal magma chambers at divergent plate boundaries. *Tectonophysics* **176**, 257–275 (1990).

123. Ernst, R. E., Grosfils, E. B. & Mege, D. Giant dike swarms: Earth, venus, and mars. *Annu. Rev. Earth Planet. Sci.* **29**, 489–534 (2001).

124. Anderson, E. M. Cone-sheets and ring-dykes: the dynamical explanation. *Bull. Volcanol.* **1**, 35–40 (1937).

125. Galland, O., Burchardt, S., Hallot, E., Mourgues, R. & Bulois, C. Dynamics of dikes versus cone sheets in volcanic systems. *J. Geophys. Res. Solid Earth* **119**, 6178–6192 (2014).

126. Gudmundsson, A. *Volcanotectonics: Understanding the Structure, Deformation and Dynamics of Volcanoes*. (Cambridge University Press, 2020).

127. Galland, O., Spacapan, J., Rabbel, O., … K. M.-J. of S. & 2019, undefined. Structure,

emplacement mechanism and magma-flow significance of igneous fingers–Implications for sill emplacement in sedimentary basins. *Elsevier*.

128. Gudmundsson, A. Emplacement and arrest of sheets and dykes in central volcanoes. *J. Volcanol. Geotherm. Res.* **116**, 279–298 (2002).

129. Galindo, I. & Gudmundsson, A. Basaltic feeder dykes in rift zones: geometry, emplacement, and effusion rates. *Nat. Hazards Earth Syst. Sci.* **12**, 3683 (2012).

130. Pollard, D. D. Elementary fracture mechanics applied to the structural interpretation of dykes. in *Mafic dyke swarms* vol. 34 5–24 (Geological Association of Canada, 1987).

131. Albino, F., Amelung, F. & Gregg, P. The role of pore fluid pressure on the failure of magma reservoirs: insights from Indonesian and Aleutian arc volcanoes. *J. Geophys. Res. Solid Earth* **123**, 1328–1349 (2018).

132. Hurwitz, D. M., Long, S. M. & Grosfils, E. B. The characteristics of magma reservoir failure beneath a volcanic edifice. *J. Volcanol. Geotherm. Res.* **188**, 379–394 (2009).

133. Delaney, P. T., Pollard, D. D., Ziony, J. I. & McKee, E. H. Field relations between dikes and joints: emplacement processes and paleostress analysis. *J. Geophys. Res. Solid Earth* **91**, 4920–4938 (1986).

134. Ziv, A. & Rubin, A. M. Static stress transfer and earthquake triggering: *J. Geophys. Res.* **105**, 13631–13642 (2000).

135. Rubin, A. M. Dikes vs. diapirs in viscoelastic rock. *Earth Planet. Sci. Lett.* **117**, 653–670 (1993).

136. Karlstrom, L., Dufek, J. & Manga, M. Magma chamber stability in arc and continental crust. *J. Volcanol. Geotherm. Res.* **190**, 249–270 (2010).

137. Gerbault, M., Hassani, R., Lizama, C. N. & Souche, A. Three-Dimensional Failure Patterns Around an Inflating Magmatic Chamber. *Wiley Online Libr.* **19**, 749–771 (2018).

138. Gregg, P. M., de Silva, S. L., Grosfils, E. B. & Parmigiani, J. P. Catastrophic caldera-forming eruptions: Thermomechanics and implications for eruption triggering and maximum caldera dimensions on Earth. *J. Volcanol. Geotherm. Res.* **241**–**242**, 1–12 (2012).

139. Terzaghi, V. K. Stress distribution in dry and in saturated sand above a yielding trap-door. in *Proceedings of the First International Conference on Soil Mechanics and Foundation Engineering* (1936).

140. Timoshenko, S. & Goodier, J. N. *Theory of Elasticity*. (McGraw-Hill, 1951).

141. Schultz, R. A. Limits on strength and deformation properties of jointed basaltic rock masses. *Rock. Mech. Rock. Engng.* **28**, 1–15 (1995).

142. Sammis, C. G. & Julian, B. R. Fracture instabilities accompanying dike intrusion. *J. Geophys. Res. Solid Earth* **92**, 2597–2605 (1987).

143. Muller, O. H. & Pollard, D. D. The stress state near Spanish Peaks, Colorado determined from a dike pattern. *Pure Appl. Geophys.* **115**, 69–86 (1977).

144. Mcleod, P. & Tait, S. The growth of dykes from magma chambers. 231–245 (1999).

145. Cañón-Tapia, E. Influence of angularities on magma tapping processes. *J. Volcanol. Geotherm. Res.* **381**, 140–156 (2019).

146. Lister, R. & Kerr, R. C. Fluid-Mechanical Models of Crack Propagation and Their Application to Magma Transport in Dykes. *J. Geophys. Res. Solid Earth* **96**, 10049–10077 (1991).

147. Dragoni, M. & Magnanensi, C. Displacement and Stress Produced by a Pressurized, Spherical Magma Chamber, Surrounded by a Viscoelastic Shell. *Phys. Earth Planet. Inter.* **56**, 316–328 (1989).

148. Segall, P. *Earthquake and volcano deformation*. (Princeton University Press, 2010). doi:10.5860/CHOICE.48-0287.

149. Bonafede, M. & Ferrari, C. Analytical models of deformation and residual gravity changes due to a Mogi source in a viscoelastic medium. *Tectonophysics* **471**, 4–13 (2009).

150. Bürgmann, R. & Dresen, G. Rheology of the lower crust and upper mantle: Evidence from rock mechanics, geodesy, and field observations. *Annu. Rev. Earth Planet. Sci.* **36**, (2008).

151. Degruyter, W. & Huber, C. A model for eruption frequency of upper crustal silicic magma chambers. *Earth Planet. Sci. Lett.* **403**, 117–130 (2014).

152. Huber, C., Townsend, M., Geoscience, W. D.-N. & 2019, undefined. Optimal depth of subvolcanic magma chamber growth controlled by volatiles and crust rheology. *nature.com*.

153. Degruyter, W., Huber, C., Bachmann, O., Cooper, K. M. & Kent, A. J. R. Influence of Exsolved Volatiles on Reheating Silicic Magmas by Recharge and Consequences for Eruptive Style at Volcán Quizapu (Chile). *Geochemistry, Geophys. Geosystems* **18**, 4123–4135 (2017).

154. Degruyter, W., Huber, C., Bachmann, O., Cooper, K. M. & Kent, A. J. R. Magma reservoir response to transient recharge events: The case of Santorini volcano (Greece). *Geology* **44**, (2015).

155. Druitt, T. *et al.* Decadal to monthly timescales of magma transfer and reservoir growth at a caldera volcano. *nature.com*.

156. Poland, M. P., Peltier, A., Bonforte, A. & Puglisi, G. The spectrum of persistent volcanic flank instability: A review and proposed framework based on K ī lauea, Piton de la Fournaise, and Etna. *J. Volcanol. Geotherm. Res.* **339**, 63–80 (2017).

157. Chaussard, E. & Amelung, F. Precursory inflation of shallow magma reservoirs at west Sunda volcanoes detected by InSAR. *Geophys. Res. Lett.* **39**, n/a—n/a (2012).

158. Biggs, J. *et al.* Global link between deformation and volcanic eruption quantified by satellite imagery. *Nat. Commun.* **5**, 1–7 (2014).
159. Singer, B. *et al.* Geomorphic expression of rapid Holocene silicic magma reservoir growth beneath Laguna del Maule, Chile. *Sci. Adv.* **4**, (2018).
160. Di Vito, M. A. *et al.* Volcanism and deformation since 12,000 years at the Campi Flegrei caldera (Italy). *J. Volcanol. Geotherm. Res.* **91**, 221–246 (1999).
161. Lundgren, P. *et al.* The dynamics of large silicic systems from satellite remote sensing observations: the intriguing case of Domuyo volcano, Argentina. *Sci. Rep.* **10**, 1–15 (2020).
162. Aiuppa, A. *et al.* The 2007 eruption of Stromboli volcano: Insights from real-time measurement of the volcanic gas plume CO2/SO2 ratio. *J. Volcanol. Geotherm. Res.* **182**, 221–230 (2009).
163. John, B. E. & Blundy, J. D. Emplacement-Related Deformation of Granitoid Magmas, Southern Adamello Massif, Italy. *Geol. Soc. Am. Bull.* **105**, 1517–1541 (1993).
164. Wiebe, R. A. & Collins, W. J. Depositional features and stratigraphic sections in granitic plutons: implications for the emplacement and crystallization of granitic magma. in *Journal of Structural Geology* 1273–1289 (1998).
165. Miller, C. F. *et al.* Growth of plutons by incremental emplacement of sheets in crystal-rich host: Evidence from Miocene intrusions of the Colorado River region, Nevada, USA. *Tectonophysics* **500**, 65–77 (2011).
166. Saunders, K. E., Morgan, D. J., Baker, J. A. & Wysoczanski, R. J. The Magmatic Evolution of the Whakamaru Supereruption, New Zealand, Constrained by a Microanalytical Study of Plagioclase and Quartz. *J. Petrol.* **51**, 2465–2488 (2010).
167. Ginibre, C. & Davidson, J. P. Sr Isotope Zoning in Plagioclase from Parinacota Volcano (Northern Chile): Quantifying Magma Mixing and Crustal Contamination. *J.*

Petrol. **55**, 1203–1238 (2014).

168. Davidson, J. P., Morgan, D. J., Charlier, B. L. A., Harlou, R. & Hora, J. M. Microsampling and Isotopic Analysis of Igneous Rocks: Implications for the Study of Magmatic Systems. *Annu. Rev. Earth Planet. Sci.* **35**, 273–311 (2007).

169. Cheng, L., Costa, F. & Bergantz, G. Linking fluid dynamics and olivine crystal scale zoning during simulated magma intrusion. *Contrib. to Mineral. Petrol.* **175**, 1–14 (2020).

170. Costa, F., Shea, T. & Ubide, T. Diffusion chronometry and the timescales of magmatic processes. *Nat. Rev. Earth Environ.* **1**, 201–214 (2020).

171. Tait, S., Jaupart, C., Letters, S. V.-E. and P. S. & 1989, undefined. Pressure, gas content and eruption periodicity of a shallow, crystallising magma chamber. *Elsevier*.

172. Liao, Y., Soule, S. A. & Jones, M. On the Mechanical Effects of Poroelastic Crystal Mush in Classical Magma Chamber Models. *J. Geophys. Res. Solid Earth* **123**, 9376–9406 (2018).

173. Zhan, Y. & Gregg, P. M. How Accurately Can We Model Magma Reservoir Failure With Uncertainties in Host Rock Rheology? *J. Geophys. Res. Solid Earth* **124**, 8030–8042 (2019).

174. Miller, C., Williams-Jones, G., … D. F.-E. and P. & 2017, undefined. 3D gravity inversion and thermodynamic modelling reveal properties of shallow silicic magma reservoir beneath Laguna del Maule, Chile. *Elsevier*.

175. Matsushima, N., Oshima, H., Ogawa, Y., … S. T.-J. of V. & 2001, undefined. Magma prospecting in Usu volcano, Hokkaido, Japan, using magnetotelluric soundings. *Elsevier*.

176. Huppert, H., Nature, A. W.- & 2002, undefined. The role of volatiles in magma chamber dynamics. *nature.com*.

177. Arzilli, F. *et al.* The unexpected explosive sub-Plinian eruption of Calbuco volcano (22-23 April 2015; southern Chile): Triggering mechanism implications. *J. Volcanol. Geotherm. Res.* 1–55 (2019).

178. Cassidy, M. *et al.* Explosive eruptions with little warning: Experimental petrology and volcano monitoring observations from the 2014 eruption of Kelud, Indonesia. *Geochemistry, Geophys. Geosystems* 2018GC008161 (2019) doi:10.1029/2018GC008161.

179. Metrich, N. & Wallace, P. J. Volatile Abundances in Basaltic Magmas and Their Degassing Paths Tracked by Melt Inclusions. *Rev. Mineral. Geochemistry* **69**, 363–402 (2008).

180. Collins, S. J., Pyle, D. M. & Maclennan, J. Melt inclusions track pre-eruption storage and dehydration of magmas at Etna. *Geology* **37**, 571–574 (2009).

181. Gaetani, G. A., O'Leary, J. A., Shimizu, N., Bucholz, C. E. & Newville, M. Rapid reequilibration of H2O and oxygen fugacity in olivine-hosted melt inclusions. *Geology* **40**, 915–918 (2012).

182. Danyushevsky, V. L., McNeill, A. W. & Sobolev, V. A. Experimental and petrological studies of melt inclusions in phenocrysts from mantle-derived magmas: An overview of techniques, advantages and complications. *Chem. Geol.* **183**, 5–24 (2002).

183. Stock, M. J. *et al.* Tracking volatile behaviour in sub-volcanic plumbing systems using apatite and glass: Insights into pre-eruptive processes at Campi Flegrei, Italy. *J. Petrol.* **59**, 2463–2492 (2018).

184. Riker, J., Humphreys, M. C. S., Brooker, R. A. & De Hoog, J. C. M. First measurements of OH-C exchange and temperature-dependent partitioning of OH and halogens in the system apatite–silicate melt. *Am. Mineral.* **103**, 260–270 (2017).

185. Blake, S. Volatile Oversaturation During the Evolution of Silicic Magma Chambers as

an Eruption Trigger. *J. Geophys. Res.* **89**, 8237–8244 (1984).

186. Scholz, C. H. *The mechanics of earthquakes and faulting*. (Cambridge University Press, 2002).

187. Avouris, D. M., Carn, S. A. & Waite, G. P. Triggering of volcanic degassing by large earthquakes. *Geology* **45**, 715–718 (2017).

188. Watters, R. J., Zimbelman, D. R., Bowman, S. D. & Crowley, J. K. Rock mass strength assessment and significance to edifice stability, Mount Rainier and Mount Hood, Cascade Range volcanoes. *Pure Appl. Geophys.* **157**, (2000).

189. Heap, M. J. *et al.* Thermal weakening of the carbonate basement under Mt. Etna volcano (Italy): Implications for volcano instability. *J. Volcanol. Geotherm. Res.* **250**, (2013).

190. Ikari, M. J., Saffer, D. M. & Marone, C. Frictional and hydrologic properties of clay-rich fault gouge. *J. Geophys. Res. Solid Earth* **114**, (2009).

191. Reid, M. E., Sisson, T. W. & Brien, D. L. Volcano collapse promoted by hydrothermal alteration and edifice shape, Mount Rainier, Washington. *Geology* **29**, (2002).

192. Farquharson, J., Heap, M. J., Baud, P., Reuschlé, T. & Varley, N. R. Pore pressure embrittlement in a volcanic edifice. *Bull. Volcanol.* **78**, (2016).

193. Paterne, M., Labeyrie, J., Guichard, F., Mazaud, A. & Maitre, F. Fluctuations of the Campanian explosive volcanic activity (SouthnItaly) during the past 190,000 years, as determined by marine tephrochronology. *Earth Planet.Sci. Lett.* **98**, 166–174 (1990).

194. Sigvaldason, G. E., Annertz, K. & Nilsson, M. Effect of glacier loading/deloading on volcanism: postglacial volcanic production rate of the Dyngjufjöll area, central Iceland. *Bull. Volcanol.* **54**, 385–392 (1992).

195. Jull, M. & McKenzie, D. The effect of deglaciation on mantle melting beneath Iceland. *J. Geophys. Res. Solid Earth* **101**, 21815–21828 (1996).

196. Jellinek, A. M., Manga, M. & Saar, M. O. Did melting glaciers cause volcanic eruptions in eastern California? Probing the mechanics of dike formation. *J. Geophys. Res. Solid Earth* **109**, 1–10 (2004).

197. Rampino, M. R. & Self, S. Climate-Volcanism Feedback and the Toba Eruption of ~74,000 Years Ago. *Quat. Res.* **40**, 269–280 (1993).

198. McGuire, W. J., Howarth, R. J., Firth, C. R. & Solow, A. R. Correlation between rate of sea-level change and frequency of explosive volcanism in the Mediterranean : Abstract : Nature. *Nature* (1997).

199. Sternai, P., Caricchi, L., Castelltort, S. & Champagnac, J. D. Deglaciation and glacial erosion: A joint control on magma productivity by continental unloading. *Geophys. Res. Lett.* **43**, (2016).

200. Kutterolf, S. *et al.* A detection of Milankovitch frequencies in global volcanic activity. *Geology* **41**, 227–230 (2013).

201. Slater, L., Jull, M., McKenzie, D. & Gronvöld, K. Deglaciation effects on mantle melting under Iceland: results from the northern volcanic zone. *Earth Planet. Sci. Lett.* **164**, 151–164 (1998).

202. Pagli, C. & Sigmundsson, F. Will present day glacier retreat increase volcanic activity? Stress induced by recent glacier retreat and its effect on magmatism at the Vatnajökull ice cap, Iceland. *Geophys. Res. Lett.* **35**, (2008).

203. Nakada, M. & Yokose, H. Ice age as a trigger of active Quaternary volcanism and tectonism. *Tectonophysics* **212**, 321–329 (1992).

204. Wilson, A. M. & Russell, J. K. Glacial pumping of a magma-charged lithosphere : A model for glaciovolcanic causality in magmatic arcs. *Earth Planet. Sci. Lett.* **548**, 116500 (2020).

205. Hooper, A. *et al.* Increased capture of magma in the crust promoted by ice-cap retreat

in Iceland. *Nat. Geosci.* **4**, 783–786 (2011).

206. Crowley, J. W., Katz, R. F., Huybers, P., LANGMUIR, C. H. & Park, S. H. Glacial cycles drive variations in the production of oceanic crust. *Science (80-.).* **347**, 1237–1240 (2015).

207. Boulahanis, B. *et al.* Do sea level variations influence mid-ocean ridge magma supply? A test using crustal thickness and bathymetry data from the East Pacific Rise. *Earth Planet. Sci. Lett.* **535**, 116121 (2020).

208. Sternai, P. *et al.* Magmatic pulse driven by sea-level changes associated with the Messinian salinity crisis. *Nat. Geosci.* **10**, 783—+ (2017).

209. Jaggar, T. A., Finch, R. H. & Emerson, O. H. THE LAVA TIDE, SEASONAL TILT, AND THE VOLCANIC CYCLE. *Mon. Wea. Rev.* **52**, 142–145 (1924).

210. Mauk, F. J. & Kienle, J. Microearthquakes at St. Augustine Volcano, Alaska, Triggered by Earth Tides. *Science (80-.).* **182**, 386–389 (1973).

211. Shimozuru, D. Lava lake oscillations and the magma reservoir beneath a volcano. *Bull. Volcanol.* **39**, 570–580 (1975).

212. Dzurisin, D. Influence of fortnightly Earth tides at Kilauea Volcano, Hawaii. *Geophys. Res. Lett.* **7**, 925–928 (1980).

213. McNutt, S. R. & Beavan, R. J. Volcanic earthquakes at Pavlof Volcano correlated with the solid earth tide. *Nature* **294**, 615–618 (1981).

214. Wilcock, W. S. D. *et al.* Seismic constraints on caldera dynamics from the 2015 Axial Seamount eruption. *Science (80-.).* **354**, 1395–1399 (2016).

215. Girona, T., Huber, C. & Caudron, C. Sensitivity to lunar cycles prior to the 2007 eruption of Ruapehu volcano. *Sci. Rep.* **8**, 1476 (2018).

216. Dinger, F. *et al.* On the link between Earth tides and volcanic degassing. *Solid Earth* **10**, 725–740 (2019).

217. Jentzsch, G., Haase, O., Kroner, C. & Winter, U. Mayon volcano, Philippines: some insights into stress balance. *J. Volcanol. Geotherm. Res.* **109**, 205–217 (2001).
218. Bredemeyer, S. & Hansteen, T. H. Synchronous degassing patterns of the neighbouring volcanoes Llaima and Villarrica in south-central Chile: the influence of tidal forces. *Int. J. Earth Sci.* **103**, 1999–2012 (2014).
219. Dinger, F. *et al.* Periodicity in the BrO⁄SO₂ molar ratios in the volcanic gas plume of Cotopaxi and its correlation with the Earth tides during the eruption in 2015. *Solid Earth* **9**, 247–266 (2018).
220. Dumont, S. *et al.* The dynamics of a long-lasting effusive eruption modulated by Earth tides. *Earth Planet. Sci. Lett.* **536**, 116145 (2020).
221. Rydelek, P. A., Sacks, I. S. & Scarpa, R. On tidal triggering of earthquakes at Campi Flegrei, Italy. *Geophys. J. Int.* **109**, 125–135 (1992).
222. Patrick, M., Swanson, D. & Orr, T. A review of controls on lava lake level: insights from Halema‘uma‘u Crater, Kīlauea Volcano. *Bull. Volcanol.* **81**, 13 (2019).
223. Neuberg, J. External modulation of volcanic activity. *Geophys. J. Int.* **142**, 232–240 (2000).
224. McNutt, S. R. & Beavan, R. J. Eruptions of Pavlof Volcano and their possible modulation by ocean load and tectonic stresses. *J. Geophys. Res. Solid Earth* **92**, 11509–11523 (1987).
225. Mason, B. G., Pyle, D. M., Dade, W. B. & Jupp, T. Seasonality of volcanic eruptions. *J. Geophys. Res. Solid Earth* **109**, (2004).
226. Kieffer, S. W. Blast dynamics at Mount St Helens on 18 May 1980. *Nature* **291**, 568–570 (1981).
227. Voight, B., Janda, R. J., Glicken, H. & Douglass, P. M. Nature and mechanics of the

Mount St Helens rockslide-avalanche of 18 May 1980. *Geotechnique* **33**, 243–273 (1983).

228. Vallance, J. W., Gardner, C. A., Scott, W. E., Iverson, R. M. & Pierson, T. C. Mount St. Helens: A 30-Year Legacy of Volcanism. *Eos, Trans. Am. Geophys. Union* **91**, 169–170 (2010).

229. Reid, M. E. *et al.* Volcano collapse promoted by progressive strength reduction: new data from Mount St. Helens. *Bull. Volcanol.* **72**, 761–7696 (2010).

230. Girona, T., Costa, F. & Schubert, G. Degassing during quiescence as a trigger of magma ascent and volcanic eruptions. *Sci. Rep.* **5**, 1–7 (2015).

231. Roman, D. C. & Cashman, V. K. Top-Down Precursory Volcanic Seismicity: Implications for 'Stealth' Magma Ascent and Long-Term Eruption Forecasting. *Front. Earth Sci.* **6**, 124 (2018).

232. Yokoyama, I. Volcanic eruptions triggered by tectonic earthquakes. *Geophys. Bull. Hokkaido Univ.* **25**, 129–139 (1971).

233. Nishimura, T. Triggering of volcanic eruptions by large earthquakes. *Geophys. Res. Lett.* **44**, 7750–7756 (2017).

234. Sawi, T. M. & Manga, M. Revisiting short-term earthquake triggered volcanism. *Bull. Volcanol.* **80**, 57 (2018).

235. Hill, D. P. *et al.* Seismicity Remotely Triggered by the Magnitude 7.3 Landers, California, Earthquake. *Science (80-.).* **260**, 1617–1623 (1993).

236. Linde, A. T. & Sacks, I. S. Triggering of volcanic eruptions. **395**, 1998 (1998).

237. Cannata, A. *et al.* Response of Mount Etna to dynamic stresses from distant earthquakes. *J. Geophys. Res. Solid Earth* **115**, (2010).

238. Yukutake, Y. *et al.* Remotely triggered seismic activity in Hakone volcano during and after the passage of surface waves from the 2011 M9.0 Tohoku-Oki earthquake. *Earth*

Planet. Sci. Lett. **373**, 205–216 (2013).

239. Hamling, I. J. & Kilgour, G. Goldilocks conditions required for earthquakes to trigger basaltic eruptions: Evidence from the 2015 Ambrym eruption. *Sci. Adv.* **6**, (2020).

240. Farías, C. & Basualto, D. Reactivating and Calming Volcanoes: The 2015 M W 8.3 Illapel Megathrust Strike. *Geophys. Res. Lett.* **47**, 1–10 (2020).

241. Pritchard, M. E., Jay, J. A., Aron, F., Henderson, S. T. & Lara, L. E. Subsidence at southern Andes volcanoes induced by the 2010 Maule, Chile earthquake. *Nat. Geosci.* **6**, 1–5 (2013).

242. Takada, Y. & Fukushima, Y. Volcanic subsidence triggered by the 2011 Tohoku earthquake in Japan. *Nat. Geosci.* **6**, 1–5 (2013).

243. Watt, S. F. L., Pyle, D. M. & Mather, T. A. The in fluence of great earthquakes on volcanic eruption rate along the Chilean subduction zone. *Earth Planet. Sci. Lett.* **277**, 399–407 (2009).

244. Prejean, S. G. & Hill, D. P. The influence of tectonic environment on dynamic earthquake triggering: A review and case study on Alaskan volcanoes. *Tectonophysics* **745**, 293–304 (2018).

245. Eggert, S. & Walter, T. R. Volcanic activity before and after large tectonic earthquakes: Observations and statistical significance. *Tectonophysics* **471**, 14–26 (2009).

246. Bebbington, M. S. & Marzocchi, W. Stochastic models for earthquake triggering of volcanic eruptions. **116**, 1–16 (2011).

247. Nostro, C., Stein, R. S., Cocco, M., Belardinelli, M. E. & Marzocchi, W. Two-way coupling between Vesuvius eruptions and southern Apennine earthquakes, Italy, by elastic stress transfer. *J. Geophys. Res. Solid Earth* **103**, 24487–24504 (1998).

248. Miyazawa, M., Nakanishi, I., Sudo, Y. & Ohkura, T. Dynamic response of frequent

tremors at Aso volcano to teleseismic waves from the 1999 Chi-Chi, Taiwan earthquake. *J. Volcanol. Geotherm. Res.* **147**, 173–186 (2005).

249. Hill, D. P. & Prejean, S. G. 4.09 - Dynamic Triggering. in *Treatise on Geophysics* (ed. Schubert, G.) 257–291 (Elsevier, 2007). doi:10.1016/B978-044452748-6.00070-5.

250. Manga, M. & Brodsky, E. Seismic Triggering of Eruptions in the Far Field: Volcanoes and Geysers . *Annu. Rev. Earth Planet. Sci.* **34**, 263–291 (2006).

251. Walter, T. R. & Amelung, F. Volcanic eruptions following M ≥ 9 megathrust earthquakes: Implications for the Sumatra-Andaman volcanoes. *Geology* **35**, 539 (2007).

252. Namiki, A. *et al.* Volcanic activities triggered or inhibited by resonance of volcanic edifices to large earthquakes. *Geology* **47**, 67–70 (2019).

253. Steinberg, G. S., Steinberg, A. S. & Merzhanov, A. G. Fluid mechanism of pressure growth in volcanic (magmatic) systems. *Mod. Geol.* **13**, 257–265 (1989).

254. Sahagian, D. L. & Proussevitch, A. A. Bubbles in volcanic systems. *Nature* **359**, 485 (1992).

255. Namiki, A., Rivalta, E., Woith, H. & Walter, T. R. Sloshing of a bubbly magma reservoir as a mechanism of triggered eruptions. *J. Volcanol. Geotherm. Res.* **320**, (2016).

256. Ujiie, K. *et al.* Low Coseismic Shear Stress on the Tohoku-Oki Megathrust Determined from Laboratory Experiments. *Science (80-.).* **342**, 1211–1214 (2013).

257. Harris, A. J. L. & Ripepe, M. Regional earthquake as a trigger for enhanced volcanic activity: Evidence from MODIS thermal data. *Geophys. Res. Lett.* **34**, (2007).

258. Walter, T. R. *et al.* Volcanic activity influenced by tectonic earthquakes: Static and dynamic stress triggering at Mt. Merapi. *Geophys. Res. Lett.* **34**, (2007).

259. Troll, V. R. *et al.* Crustal CO2 liberation during the 2006 eruption and earthquake

events at Merapi volcano, Indonesia. *Geophys. Res. Lett.* **39**, (2012).

260. Carr, B. B., Clarke, A. B. & de' Michieli Vitturi, M. Earthquake induced variations in extrusion rate: A numerical modeling approach to the 2006 eruption of Merapi Volcano (Indonesia). *Earth Planet. Sci. Lett.* **482**, 377–387 (2018).

261. White, R. & Mccausland, W. Volcano-tectonic earthquakes: A new tool for estimating intrusive volumes and forecasting eruptions. *J. Volcanol. Geotherm. Res.* **309**, 139–155 (2016).

262. Toda, S., Stein, R. S. & Sagiya, T. Evidence from the AD 2000 Izu islands earthquake swarm that stressing rate governs seismicity. *Nature* **419**, 58–61 (2002).

263. Xu, W., Jonsson, S., Corbi, F. & Rivalta, E. Graben formation and dike arrest during the 2009 Harrat Lunayyir dike intrusion in Saudi Arabia: Insights from InSAR, stress calculations and analog experiments. *J. Geophys. Res. Solid Earth* **121**, 2837–2851 (2016).

264. Bonaccorso, A., Aoki, Y. & Rivalta, E. Dike propagation energy balance from deformation modeling and seismic release. *Geophys. Res. Lett.* **44**, (2017).

265. Talwani, P. & Acree, S. Pore pressure diffusion and the mechanism of reservoir-induced seismicity. *pure appl. Geophys.* **122**, 547–965 (1984).

266. Saar, M. O. & Manga, M. Seismicity induced by seasonal groundwater recharge at Mt. Hood, Oregon. *Earth Planet. Sci. Lett.* **214**, 605–618 (2003).

267. Keranen, K. M., Weingarten, M., Abers, G. A., Bekins, B. A. & Ge, S. Sharp increase in central Oklahoma seismicity since 2008 induced by massive wastewater injection. *Science (80-.).* **345**, 448–451 (2014).

268. Violette, S. *et al.* Can rainfall trigger volcanic eruptions? A mechanical stress model of an active volcano: Piton de la Fournaise, Reunion Island. *Terra Nov.* **13**, 18–24 (2001).

269. Farquharson, J. I. & Amelung, F. Extreme rainfall triggered the 2018 rift eruption at

Kīlauea Volcano. *Nature* **580**, 491–495 (2020).

270. Hort, M., Seyfried, R. & Vöge, M. Radar Doppler velocimetry of volcanic eruptions: theoretical considerations and quantitative documentation of changes in eruptive behaviour at Stromboli volcano, Italy. *Geophys. J. Int.* **154**, 515–532 (2003).

271. Manga, M. When it rains , lava pours. *Nat. News Views* **580**, 457–458 (2020).

272. Richter, G., Wassermann, J., Zimmer, M. & Ohrnberger, M. Correlation of seismic activity and fumarole temperature at the Mt. Merapi volcano (Indonesia) in 2000. *J. Volcanol. Geotherm. Res.* **135**, 331–342 (2004).

273. Matthews, A. J., Barclay, J. & Johnstone, J. E. The fast response of volcano-seismic activity to intense precipitation: Triggering of primary volcanic activity by rainfall at Soufrière Hills Volcano, Montserrat. *J. Volcanol. Geotherm. Res.* **184**, 405–415 (2009).

274. Matthews, A. J. Rainfall-induced volcanic activity on Montserrat. *Geophys. Res. Lett.* **29**, 1644 (2002).

275. Carn, S. A., Watts, R. B., Thompson, G. & Norton, G. E. Anatomy of a lava dome collapse: the 20 March 2000 event at Soufrière Hills Volcano, Montserrat. *J. Volcanol. Geotherm. Res.* **131**, 241–264 (2004).

276. Yamasato, H., Kitagawa, S. & Komiya, M. Effect of rainfall on dacitic lava dome collapse at Unzen volcano, Japan. *Pap. Meteorol. Geophys.* **48**, 73–78 (1998).

277. Voight, B., Constantine, E. K., Siswowidjoyo, S. & Torley, R. Historical eruptions of Merapi Volcano, Central Java, Indonesia, 1768–1998. *J. Volcanol. Geotherm. Res.* **100**, 69–138 (2000).

278. MASTIN, L. G. Explosive tephra emissions at Mount St. Helens, 1989-1991: The violent escape of magmatic gas following storms? *Geol. Soc. Am. Bull.* **106**, 175–185 (1994).

279. Gaete, A. *et al.* Processes culminating in the 2015 phreatic explosion at Lascar volcano, Chile, evidenced by multiparametric data. *Nat. Hazards Earth Syst. Sci.* **20**, 377–397 (2020).

280. López, D. L. & Williams, S. N. Catastrophic volcanic collapse: Relation to hydrothermal processes. *Science (80-.).* **260**, (1993).

281. Voight, B. & Elsworth, D. Instability and collapse of hazardous gas-pressurized lava domes. *Geophys. Res. Lett.* **27**, 1–4 (2000).

282. Gonnermann, H. M. & Manga, M. The fluid mechanics inside a volcano. *Annual Review of Fluid Mechanics* vol. 39 321–356 (2007).

283. Costa, A., Melnik, O. & Sparks, R. S. J. Controls of conduit geometry and wallrock elasticity on lava dome eruptions. *Earth Planet. Sci. Lett.* **260**, (2007).

284. Of, J., Research ; Anderson, G. & Segall, P. Bayesian inversion of data from effusive volcanic eruptions using physics-based models: Application to Mount St. *J. Geophys. Res. Solid Earth* **118**, 2017–2019 (2013).

285. Massaro, S., Costa, A., Letters, R. S.-E. and P. S. & 2018, undefined. Evolution of the magma feeding system during a Plinian eruption: The case of Pomici di Avellino eruption of Somma–Vesuvius, Italy. *Elsevier*.

286. Landi, P., Marchetti, E., La Felice, S., Ripepe, M. & Rosi, M. Integrated petrochemical and geophysical data reveals thermal distribution of the feeding conduits at Stromboli volcano, Italy. *Geophys. Res. Lett.* **38**, (2011).

287. Acocella, V. *et al.* Why does a mature volcano need new vents? The case of the new Southeast crater at Etna. *Front. Earth Sci.* **4**, (2016).

288. Pering, T. *et al.* Combined ground and aerial measurements resolve vent-specific gas fluxes from a multi-vent volcano. *nature.com*.

289. Rivalta, E. *et al.* Stress inversions to forecast magma pathways and eruptive vent

location. *Sci. Adv.* **5**, (2019).

290. Griffith, A. A. The phenomena of rupture and flow in solids. *Philos. Trans. R. Soc. A Math. Phys. Eng. Sci.* **221**, (1921).

291. Irwin, G. R. *Onset of fast crack propagation in high strength steel and aluminum alloys*. (1956).

292. Nakashima, Y. *Static Stability and Propagation of a Fluid-Filled Edge Crack in Rock: Implication for Fluid Transport in Magmatism and Metamorphism*. *J. Phys. Earth* vol. 41 https://www.jstage.jst.go.jp/article/jpe1952/41/3/41_3_189/_article/-char/ja/ (1993).

293. Buck, W. R., Einarsson, P. & Brandsdóttir, B. Tectonic stress and magma chamber size as controls on dike propagation: Constraints from the 1975-1984 Krafla rifting episode. *J. Geophys. Res. Solid Earth* **111**, (2006).

294. Grandin, R., Socquet, A., Doubre, C., … E. J.-E. and P. & 2012, undefined. Elastic thickness control of lateral dyke intrusion at mid-ocean ridges. *Elsevier*.

295. Weertman, J. *Theory of Water-Filled Crevasses in Glaciers Applied to Vertical Magma Transport beneath Oceanic Ridges*. *Wiley Online Library* vol. 76 https://agupubs.onlinelibrary.wiley.com/doi/abs/10.1029/JB076i005p01171?casa_token=UUWmUiO5n50AAAAA:IwF39zkCO1PKFHveTUw_d8hyIyUAPdlmKzWx2RBzdpw77_EsRMj1YXqQ_GpapThmv0i-T9FjnyfIVUn_ (1971).

296. Secor, D. T. & Pollard, D. D. On the stability of open hydraulic fractures in the Earth's crust. *Geophys. Res. Lett.* **2**, 510–513 (1975).

297. Rubin, A. M., Gillard, D. & Luc, J.-. *A reinterpretation of seismicity associated with the January 1983 dike intrusion at Kilauea Volcano, Hawaii*. *JOURNAL OF GEOPHYSICAL RESEARCH* vol. 103 https://agupubs.onlinelibrary.wiley.com/doi/abs/10.1029/97JB03513 (1998).

298. Geshi, N., Kusumoto, S., and, A. G.-J. of V. & 2012, undefined. Effects of mechanical

layering of host rocks on dike growth and arrest. *Elsevier*.

299. Kervyn, M., Ernst, G. G. J., van Wyk de Vries, B., Mathieu, L. & Jacobs, P. Volcano load control on dyke propagation and vent distribution: Insights from analogue modeling. *J. Geophys. Res.* **114**, B03401 (2009).

300. Rivalta, E. & Dahm, T. Acceleration of buoyancy-driven fractures and magmatic dikes beneath the free surface. *Geophys. J. Int.* **166**, (2006).

301. Anderson, E. M. The dynamics of faulting and dyke formation with applications to Britain. (1951).

302. Maccaferri, F., Acocella, V. & Rivalta, E. How the differential load induced by normal fault scarps controls the distribution of monogenic volcanism. *Wiley Online Libr.* **42**, 7507–7512 (2015).

303. Dahm, T. Numerical simulations of the propagation path and the arrest of fluid-filled fractures in the Earth. *Geophys. J. Int.* **141**, 623–638 (2000).

304. Maccaferri, F., Bonafede, M. & Rivalta, E. A quantitative study of the mechanisms governing dike propagation, dike arrest and sill formation. *J. Volcanol. Geotherm. Res.* **208**, 39–50 (2011).

305. Heimisson, E. R., Hooper, A. & Sigmundsson, F. Forecasting the path of a laterally propagating dike. *J. Geophys. Res. Solid Earth* **120**, 8774–8792 (2015).

306. Zoback, L. M. *et al.* Global patterns of tectonic stress. *Nature* **341**, 291–298 (1989).

307. Grosfils, E., McGovern, P., … P. G.-G. S. & 2015, undefined. Elastic models of magma reservoir mechanics: a key tool for investigating planetary volcanism. *sp.lyellcollection.org*.

308. Muller, J. R., Ito, G. & Martel, S. J. Effects of volcano loading on dike propagation in an elastic half-space load. *J. Geophys. Res.* **106**, 11101–11113 (2001).

309. Watanabe, T., Masuyama, T., Nagaoka, K. & Tahara, T. Analog experiments on

magma-filled cracks : Competition between external stresses and internal pressure. *Earth, Planets Sp.* **54**, 1247–1261 (2002).

310. Maccaferri, F., Smittarello, D., Pinel, V. & Cayol, V. On the Propagation Path of Magma Filled Dikes and Hydrofractures: The Competition Between External Stress , Internal Pressure, and Crack Length. *Geochemistry Geophys. Geosystems* **20**, 2064–2081 (2019).

311. Dieterich, J. H. Growth and persistence of Hawaiian volcanic rift zones. *J. Geophys. Res.* **93**, 4258–4270 (1988).

312. Chadwick, W. W. & Dieterich, J. H. Mechanical modeling of circumferential and radial dike intrusion on Galapagos volcanoes. *J. Volcanol. Geotherm. Res.* **66**, 37–52 (1995).

313. Acocella, V. & Neri, M. Dike propagation in volcanic edifices: Overview and possible developments. *Tectonophysics* **471**, 67–77 (2009).

314. Thiele, S. T., Cruden, A. R., Micklethwaite, S., Bunger, A. P. & Köpping, J. Dyke apertures record stress accumulation during sustained volcanism. *Sci. Rep.* 1–9 (2020) doi:10.1038/s41598-020-74361-w.

315. McGuire, W. J. & Pullen, A. D. Location and orientation of eruptive fissures and feederdykes at Mount Etna; influence of gravitational and regional tectonic stress regimes. *J. Volcanol. Geotherm. Res.* (1989) doi:10.1016/0377-0273(89)90046-2.

316. Delcamp, A., van Wyk de Vries, B. & James, M. R. The influence of edifice slope and substrata on volcano spreading. *J. Volcanol. Geotherm. Res.* (2008) doi:10.1016/j.jvolgeores.2008.07.014.

317. Urbani, S., Acocella, V., Rivalta, E. & Corbi, F. Propagation and arrest of dikes under topography: Models applied to the 2014 Bardarbunga (Iceland) rifting event. *Geophys. Res. Lett.* **44**, 6692–6701 (2017).

318. Peltier, A., Ferrazzini, V., Staudacher, T. & Bachèlery, P. Imaging the dynamics of dyke propagation prior to the 2000-2003 flank eruptions at Piton de la Fournaise, Reunion Island. *Geophys. Res. Lett.* **32**, 1–5 (2005).

319. Townsend, M. R., Pollard, D. D. & Smith, R. P. Mechanical models for dikes: A third school of thought. *Tectonophysics* **703–704**, 98–118 (2017).

320. Hjartardóttir, Á. R. & Einarsson, P. The interaction of fissure swarms and monogenetic lava shields in the rift zones of Iceland. *J. Volcanol. Geotherm. Res.* **299**, 91–102 (2015).

321. Ventura, G., Vilardo, G. & Bruno, P. P. The role of flank failure in modifying the shallow plumbing system of volcanoes: an example from Somma-Vesuvius, Italy, lava flows. *Geophys. Res. Lett.* **26**, 3681–3684 (1999).

322. Corbi, F. *et al.* How caldera collapse shapes the shallow emplacement and transfer of magma in active volcanoes. *Earth Planet. Sci. Lett.* **431**, 287–293 (2015).

323. Galetto, F., Acocella, V., communications, L. C.-N. & 2017, undefined. Caldera resurgence driven by magma viscosity contrasts. *nature.com*.

324. Heidbach, O., Rajabi, M., Reiter, K., … M. Z.-G. D. & 2016, undefined. World stress map database release 2016. *researchgate.net*.

325. Mantiloni, L., Davis, T., Rojas, A. B. G. & Rivalta, E. Stress inversion in a gelatin box: testing eruptive vent location forecasts with analog models. *Geophys. Res. Lett.* (2021) doi:10.1029/2020GL090407.

326. Tibaldi, A. Structure of volcano plumbing systems: A review of multi-parametric effects. *Journal of Volcanology and Geothermal Research* vol. 298 (2015).

327. Segall, P. Magma chambers: what we can, and cannot, learn from volcano geodesy. *royalsocietypublishing.org* **377**, (2019).

328. Anderson, K., Johanson, I., Patrick, M., … M. G.- & 2019, undefined. Magma

reservoir failure and the onset of caldera collapse at Kīlauea Volcano in 2018. *science.sciencemag.org*.

329. Paulatto, M. *et al.* Vertically Extensive Magma Reservoir Revealed From Joint Inversion and Quantitative Interpretation of Seismic and Gravity Data. *J. Geophys. Res. Solid Earth* **124**, (2019).

330. Pollard, D., Geology, M. T.-J. of S. & 2018, undefined. Fluid-filled fractures in Earth's lithosphere: gravitational loading, interpenetration, and stable height of dikes and veins. *Elsevier*.

331. Maimon, O., Lyakhovsky, V., … O. M.-G. J. & 2012, undefined. The propagation of a dyke driven by gas-saturated magma. *academic.oup.com*.

332. Heap, M. J. *et al.* Mechanical behaviour and failure modes in the Whakaari (White Island volcano) hydrothermal system, New Zealand. *J. Volcanol. Geotherm. Res.* **295**, 26–42 (2015).

333. Crosweller, H. S. *et al.* Global database on large magnitude explosive volcanic eruptions (LaMEVE). *J. Appl. Volcanol.* **1**, (2012).

334. Marxer, F. & Ulmer, P. Crystallisation and zircon saturation of calc alkaline tonalite from the Adamello Batholith at upper crustal conditions : an experimental study. *Contrib. to Mineral. Petrol.* (2019) doi:10.1007/s00410-019-1619-x.

335. Lesher, C., volcanoes, F. S.-T. encyclopedia of & 2015, undefined. Thermodynamic and transport properties of silicate melts and magma. *Elsevier*.

336. Matzel, J. E. P., Bowring, S. A. & Miller, R. B. Time scales of pluton construction at differing crustal levels: Examples from the Mount Stuart and Tenpeak intrusions, North Cascades, Washington. *Geol. Soc. Am. Bull.* **118**, 1412–1430 (2006).

337. Menand, T., Annen, C. & de Saint-Blanquat, M. Rates of magma transfer in the crust: Insights into magma reservoir recharge and pluton growth. *Geology* **43**, 199–202

(2015).

338. Rutter, E. H. & Brodie, K. H. Experimental intracrystalline plastic flow in hot-pressed synthetic quartzite prepared from Brazilian quartz crystals. *J. Struct. Geol.* **26**, 259–270 (2004).

339. Rybacki, E. & Dresen, G. Dislocation and diffusion creep of synthetic anorthite aggregates. *J. Geophys. Res. Solid Earth* **105**, 26017–26036 (2000).

340. Zielinski, R. A. & Lipman, P. W. Trace-element variations at Summer Coon volcano, San Juan Mountains, Colorado, and the origin of continental-interior andesite. *Bull. Geol. Soc. Am.* (1976) doi:10.1130/0016-7606(1976)871477:TVASCV2.0.CO;2.

341. Burchardt, S., Troll, V. R., Mathieu, L., Emeleus, H. C. & Donaldson, C. H. Ardnamurchan 3D cone-sheet architecture explained by a single elongate magma chamber. *Sci. Rep.* **3**, (2013).

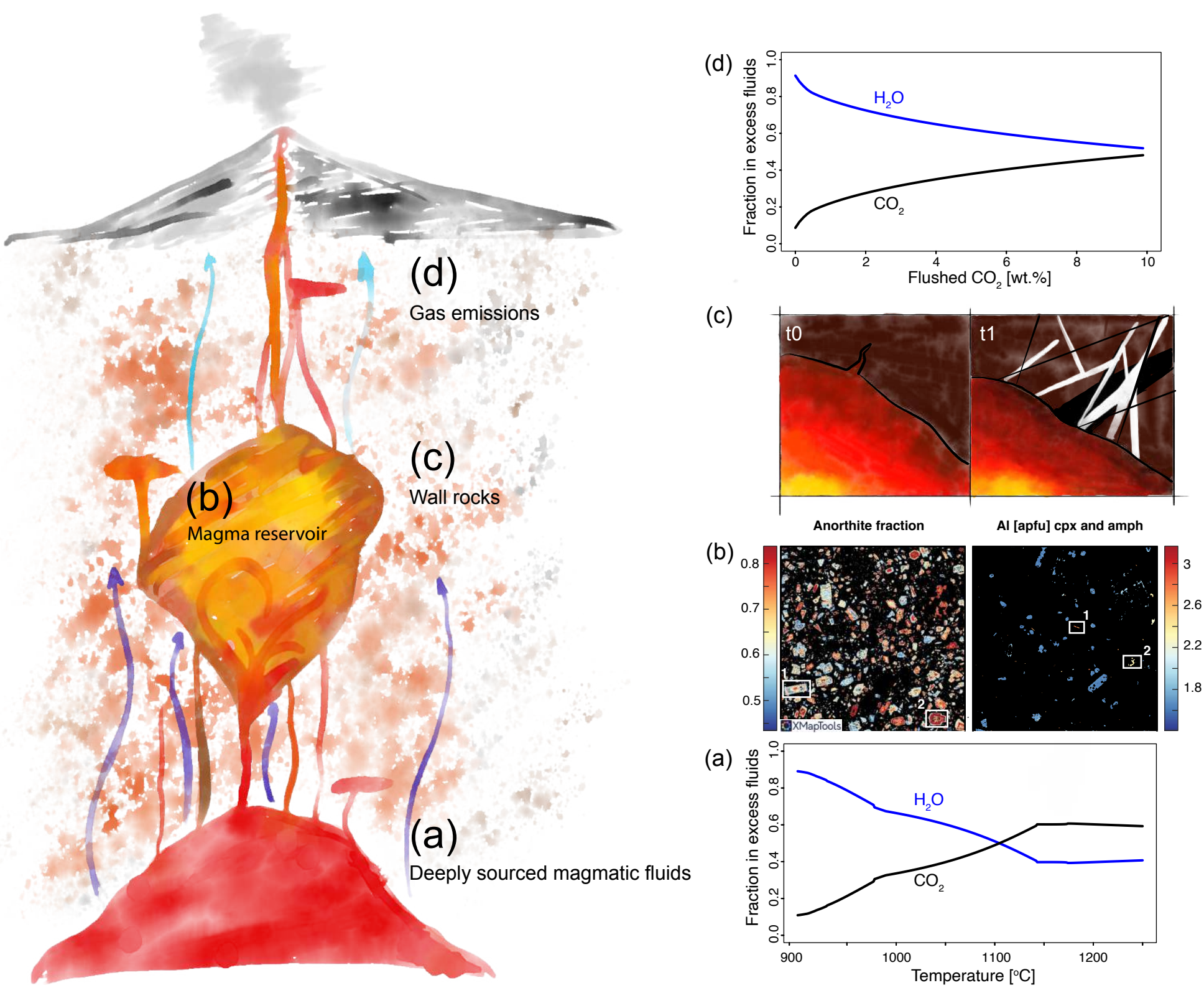
(d)
Gas emissions
(c)
Wall rocks
(b)
Magma reservoir
(a)
Deeply sourced magmatic fluids

(d)
Fraction in excess fluids
H2O
CO2
Flushed CO2 [wt.%]

(c)
t0
t1
Anorthite fraction
Al [apfu] cpx and amph

(b)
XMapTools

(a)
Fraction in excess fluids
H2O
CO2
Temperature [°C]

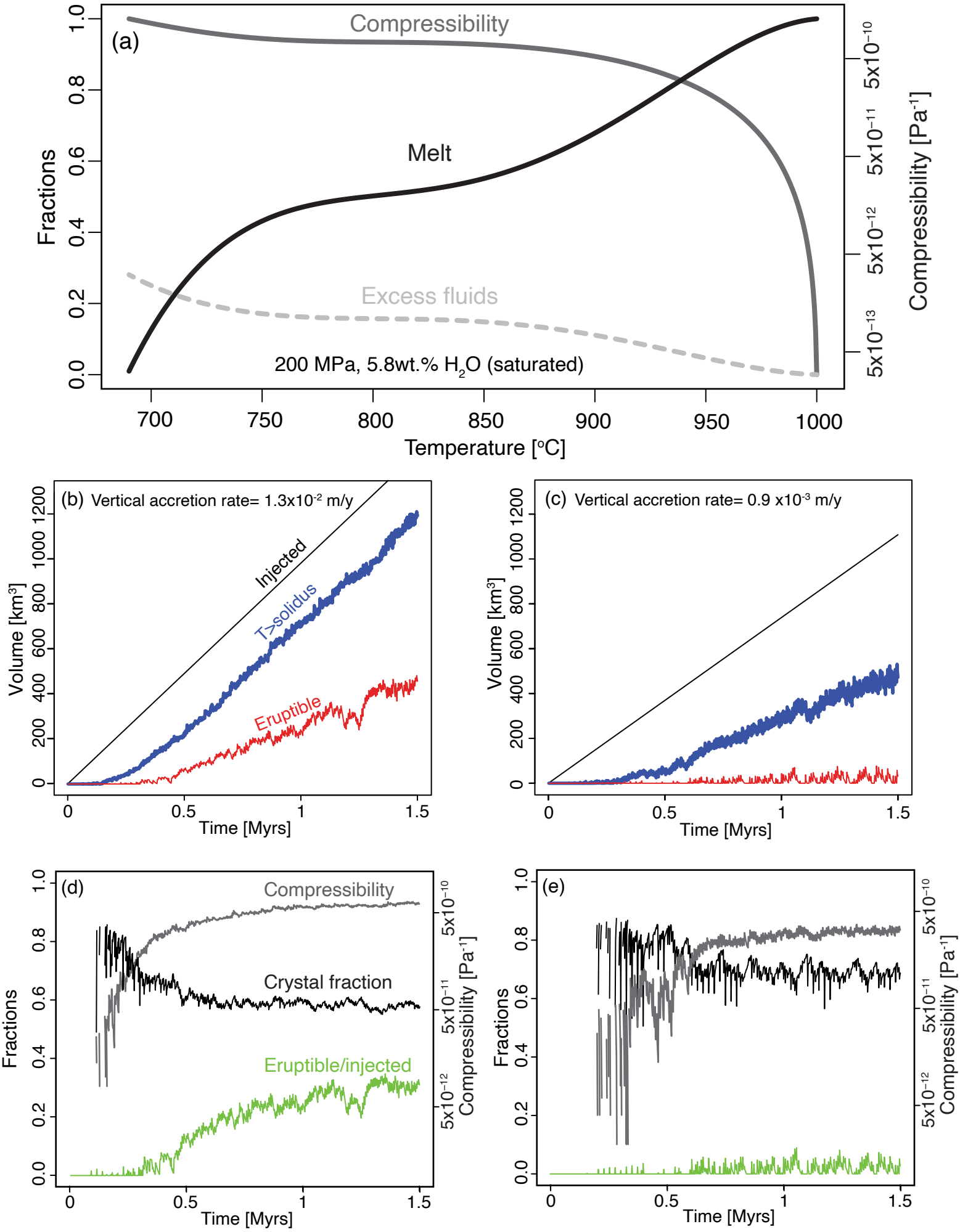
(a)
Compressibility
Melt
Excess fluids
200 MPa, 5.8wt.% H2O (saturated)
Fractions
Compressibility [Pa-1]
Temperature [oC]
(b) Vertical accretion rate= 1.3x10-2 m/y
Injected
T>solidus
Eruptible
Volume [km3]
Time [Myrs]
(c) Vertical accretion rate= 0.9 x10-3 m/y
Volume [km3]
Time [Myrs]
(d)
Compressibility
Crystal fraction
Eruptible/injected
Fractions
Compressibility [Pa-1]
Time [Myrs]
(e)
Fractions
Compressibility [Pa-1]
Time [Myrs]

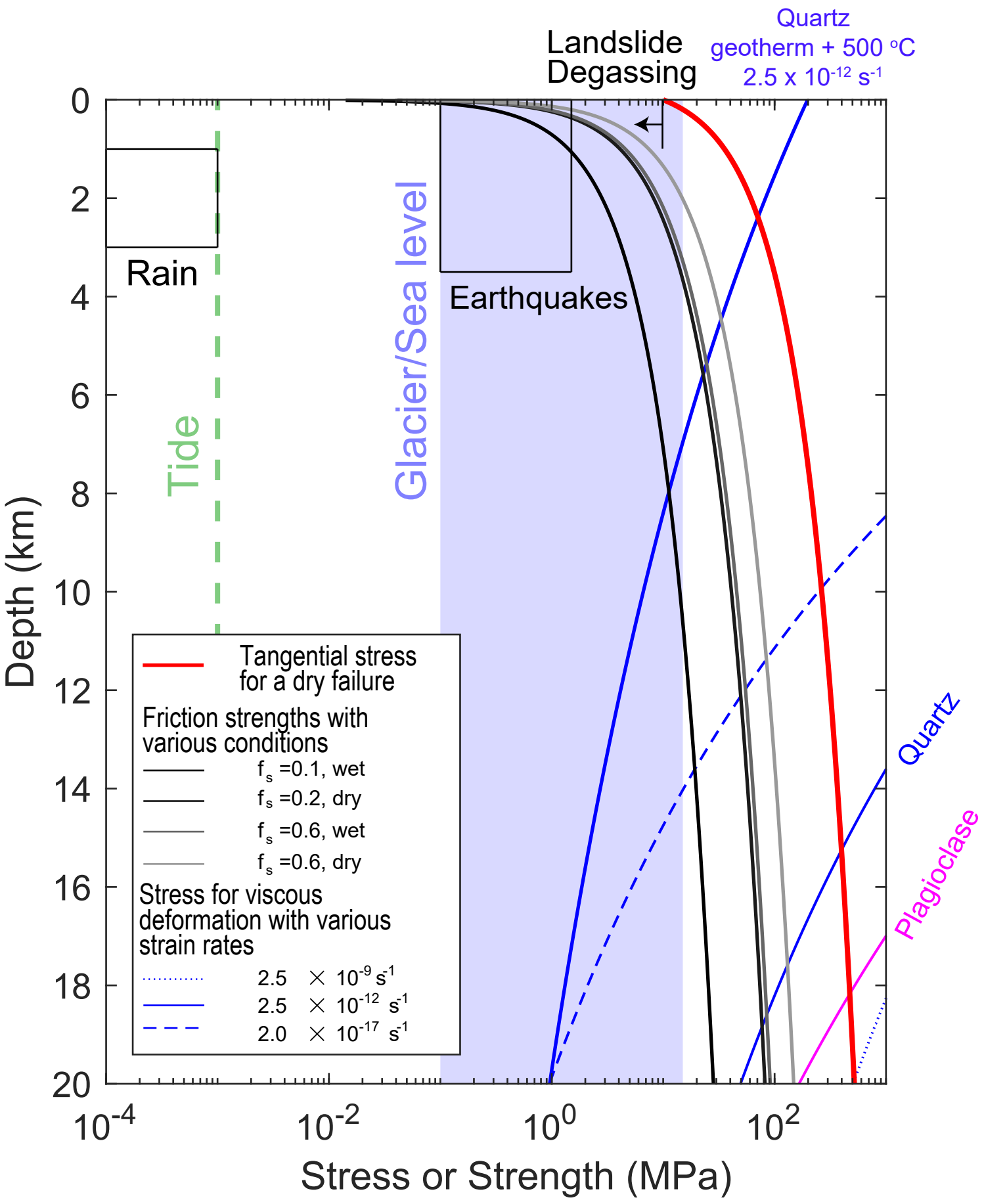
Landslide
Degassing
Quartz
geotherm + 500 °C
2.5 x 10-12 s-1
Rain
Earthquakes
Tide
Glacier/Sea level
Depth (km)
0
2
4
6
8
10
12
14
16
18
20
10-4
10-2
100
102
Stress or Strength (MPa)
Tangential stress
for a dry failure
Friction strengths with
various conditions
fs =0.1, wet
fs =0.2, dry
fs =0.6, wet
fs =0.6, dry
Stress for viscous
deformation with various
strain rates
2.5 × 10-9 s-1
2.5 × 10-12 s-1
2.0 × 10-17 s-1
Quartz
Plagioclase

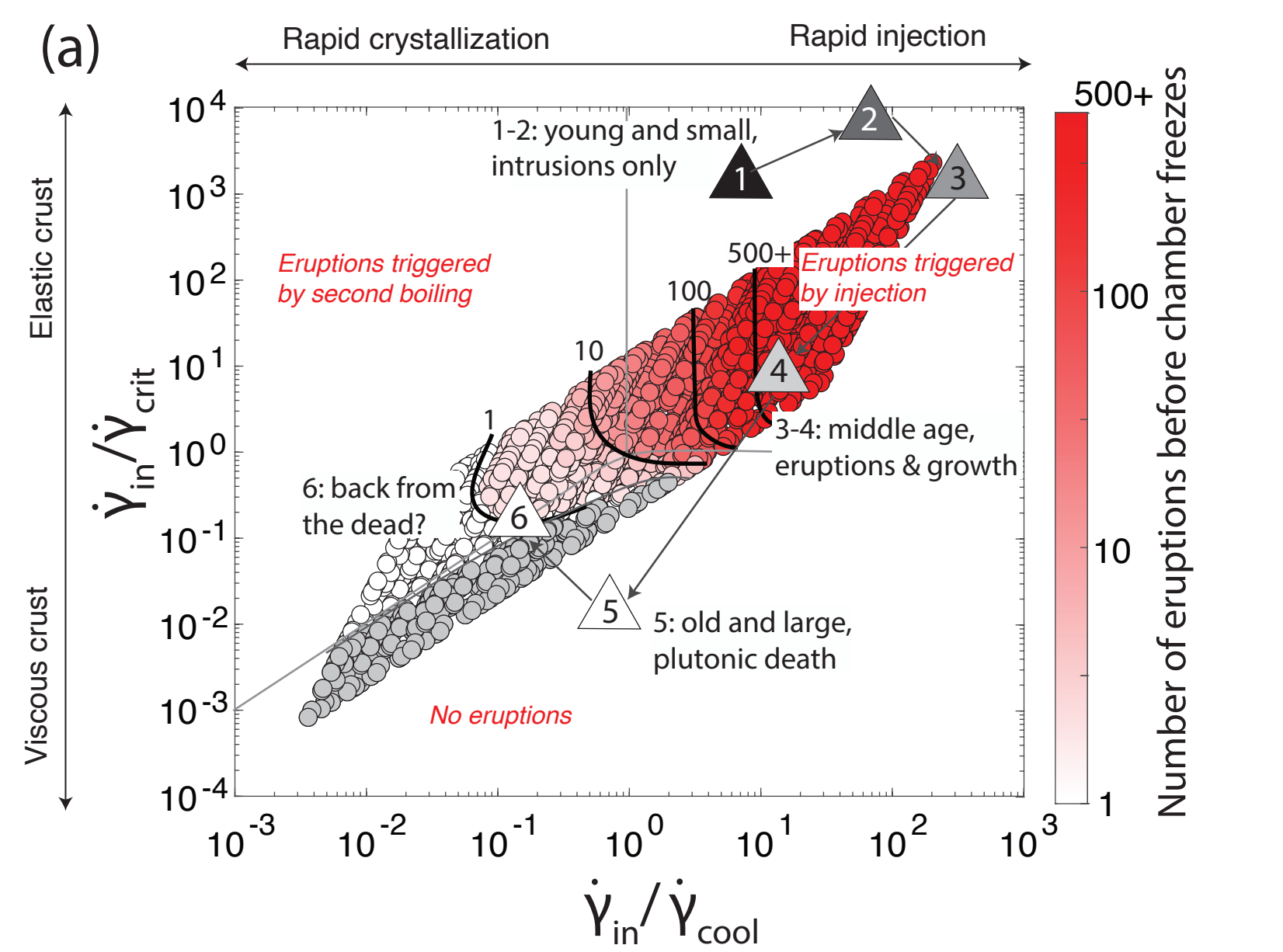
(a)
Rapid crystallization
Rapid injection
Elastic crust
Viscous crust
$\dot{\gamma}_{in}/\dot{\gamma}_{crit}$
$\dot{\gamma}_{in}/\dot{\gamma}_{cool}$
1-2: young and small, intrusions only
Eruptions triggered by second boiling
Eruptions triggered by injection
3-4: middle age, eruptions & growth
6: back from the dead?
5: old and large, plutonic death
No eruptions
500+
100
10
1
Number of eruptions before chamber freezes

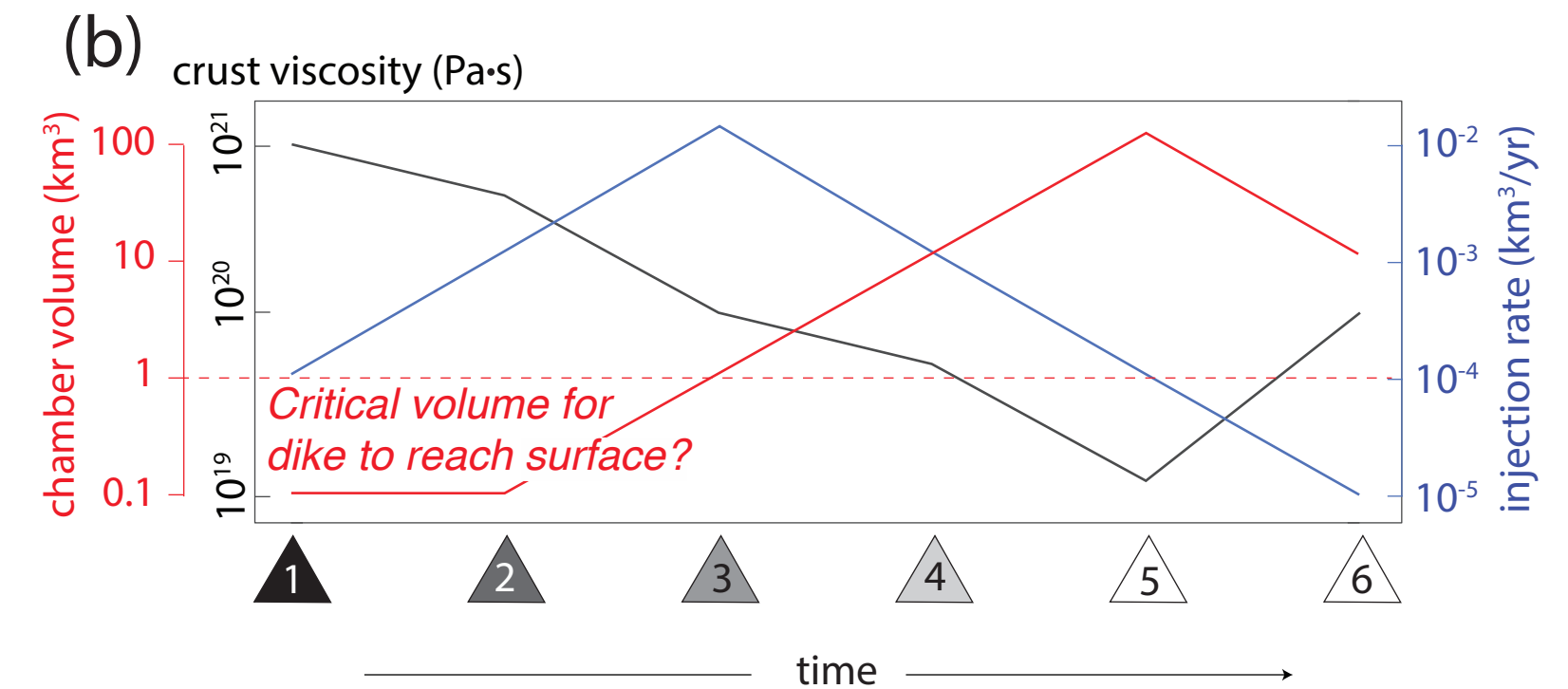
(b)
crust viscosity (Pa•s)
chamber volume (km³)
injection rate (km³/yr)
Critical volume for dike to reach surface?
time

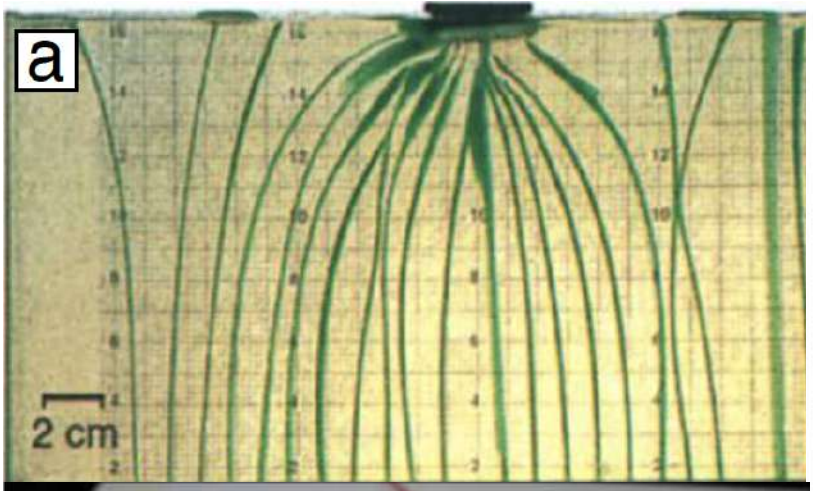
a
2 cm


b

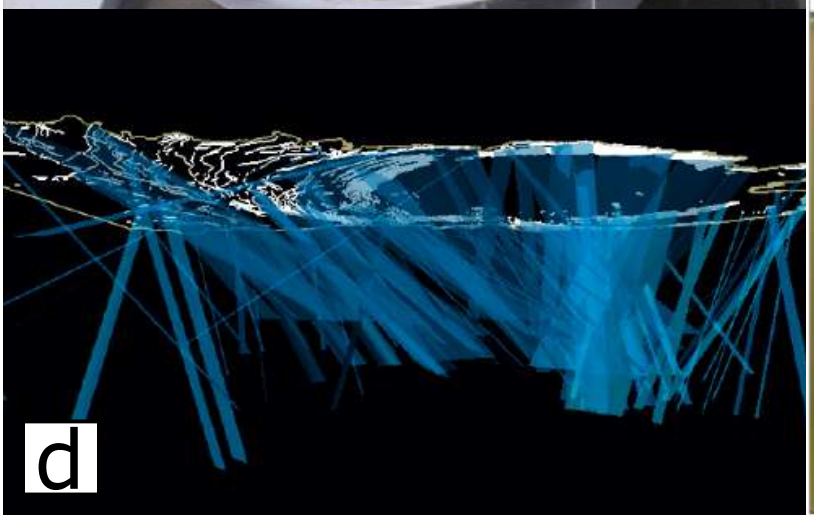
d

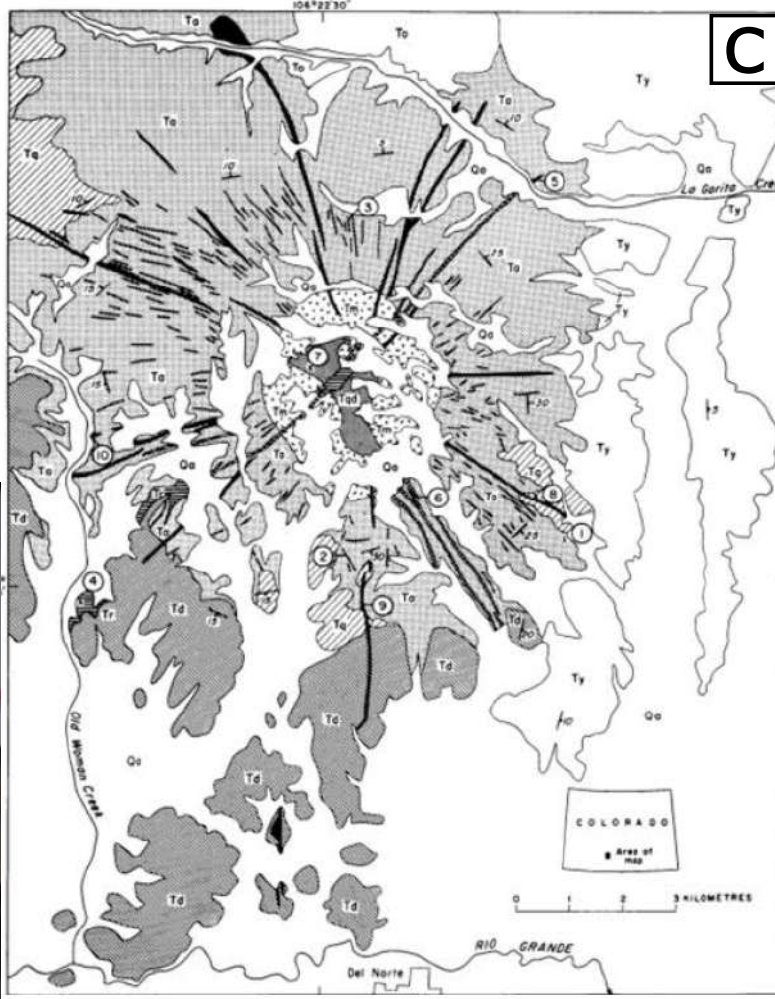
c
106°22'30"
Ta
Ty
Qa
La Garita
Cre
Td
Tg
Tz
Old Woman Creek
COLORADO
Area of map
0 1 2 3 KILOMETRES
RIO GRANDE
Del Norte


e

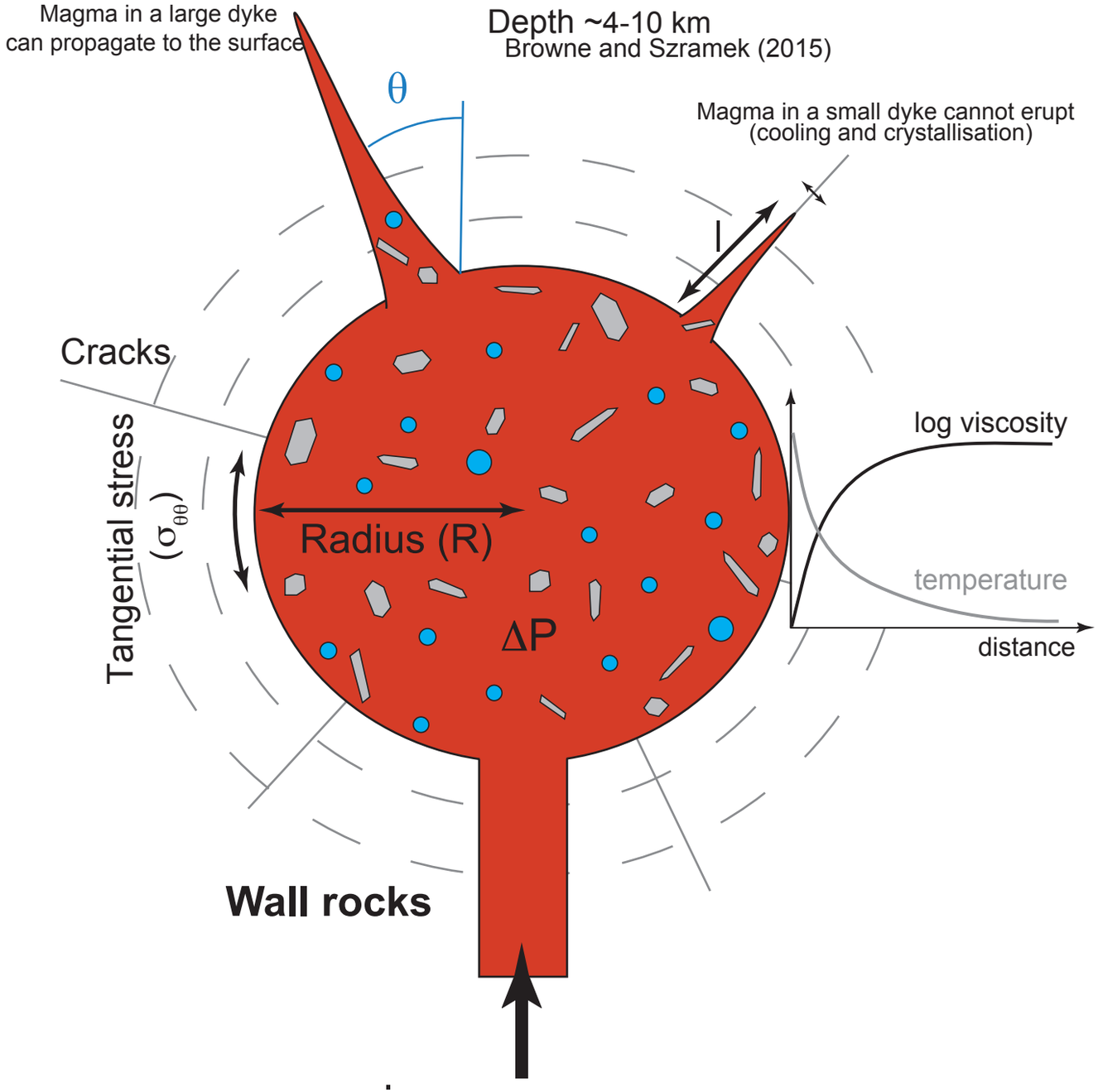

Wall rocks

Viscosity (η_r) [Pa·s]: 10^{19}-10^{21} Bürgmann and Dresen (2008)
Shear Modulus (μ) [Pa]: 10^{10} Schultz (1995)
Relaxation time (η_r/μ) [yrs]: 10-1000
Fracture toughness (K_c) [MPa m$^{1/2}$]: 1-10 Rubin (1995)
Tensile strength (Ts): 1-100 MPa Schultz (1995)

Magma reservoir e.g., Lesher and Spera (2015)

Viscosity (η_m) [Pa·s]
Mafic: 1-10
Felsic: >10^3

Strain rate: $\frac{1}{R}\frac{dR}{dt}$

Overpressure (ΔP): $\frac{\Delta V}{V}\beta^{-1}$